Comparison of radiation dose and image quality between fast kVp switching dual-energy CT and routine single-energy CT for whole abdomen at King Chulalongkorn Memorial Hospital

Miss Chanthawan Khemkhangboon

A Thesis Submitted in Partial Fulfillment of the Requirements
for the Degree of Master of Science in Medical Physics
Department of Radiology
FACULTY OF MEDICINE
Chulalongkorn University
Academic Year 2022
Copyright of Chulalongkorn University

การเปรียบเทียบปริมาณรังสีและคุณภาพของภาพระหว่างเอกซเรย์คอมพิวเตอร์สองพลังงานชนิด
สลับค่าความต่างศักย์สูงสุดอย่างรวดเร็วและพลังงานค่าเดียวสำหรับช่องท้องทั้งหมด ณ
โรงพยาบาลจุฬาลงกรณ์ สภากาชาดไทย

น.ส.จันทวรรณ เข้มแข็งบุญ

Thesis Title	Comparison of radiation dose and image quality between fast kVp switching dual-energy CT and routine single-energy CT for whole abdomen at King Chulalongkorn Memorial Hospital
By	Miss Chanthawan Khemkhangboon
Field of Study	Medical Physics
Thesis Advisor	Assistant Professor KITIWAT KHAMWAN, Ph.D.

Accepted by the FACULTY OF MEDICINE, Chulalongkorn University in Partial Fulfillment of the Requirement for the Master of Science

.... Dean of the FACULTY OF MEDICINE

(Associate Professor CHANCHAI SITTIPUNT, M.D.)

THESIS COMMITTEE

.... Chairman

(Associate Professor ANCHALI KRISANACHINDA, Ph.D.)

.... Thesis Advisor

(Assistant Professor KITIWAT KHAMWAN, Ph.D.)

.... External Examiner

(Professor Kosuke Matsubara, Ph.D.)

จุฬาลงกรณ์มหาวิทยาลัย

CHULALONGKORN UNIVERSITY

จันทวรรณ เข้มแข็งบุญ : การเปรียบเทียบปริมาณรังสีและคุณภาพของภาพระหว่างเอกซเรย์คอมพิวเตอร์สองพลังงานชนิดสลับค่าความต่างศักย์สูงสุดอย่างรวดเร็วและพลังงานค่าเดียวสำหรับช่องท้องทั้งหมด ณ โรงพยาบาลจุฬาลงกรณ์ สภากาชาดไทย. (Comparison of radiation dose and image quality between fast kVp switching dual-energy CT and routine single-energy CT for whole abdomen at King Chulalongkorn Memorial Hospital) อ.ที่ปรึกษาหลัก : ผศ. ดร.กิติวัฒน์ คำวัน

การตรวจเอกซเรย์คอมพิวเตอร์ช่องท้องโดยใช้รังสีเอกซ์พลังงานเดียวเป็นขั้นตอนการถ่ายภาพทั่วไปในโรงพยาบาล อย่างไรก็ตามด้วยวิวัฒนาการของเทคโนโลยีเอกซเรย์คอมพิวเตอร์สองพลังงานได้เริ่มพัฒนามากขึ้น เครื่องเอกซเรย์คอมพิวเตอร์สองพลังงานชนิดสลับค่าความต่างศักย์สูงสุดอย่างรวดเร็วได้รับการติดตั้งที่โรงพยาบาลจุฬาลงกรณ์ในปี พ.ศ. 2560 และยังไม่มีการศึกษาประโยชน์ทางคลินิกในผู้ป่วยฉุกเฉิน ดังนั้นการศึกษานี้มีวัตถุประสงค์เพื่อต้องการเปรียบเทียบปริมาณรังสีและคุณภาพของภาพเอกซเรย์คอมพิวเตอร์ระหว่างรังสีเอกซ์พลังงานเดียวและสองพลังงานของการตรวจเอกซเรย์คอมพิวเตอร์ช่องท้องทั้งหมดสำหรับผู้ป่วยฉุกเฉิน ทำการรวบรวมข้อมูลเอกซเรย์คอมพิวเตอร์ย้อนหลังจากผู้ป่วยขนาดมาตรฐาน 130 รายที่ได้รับการฉีดสารทึบรังสีจากเครื่องเอกซเรย์คอมพิวเตอร์ 256 สไลซ์ โดยใช้เวลา 70 วินาทีในการฉีดสารทึบรังสีชนิดไอโอบิทริดอลโดยใช้เครื่องฉีดยาอัตโนมัติในอัตรา 2 มล./วินาที ผ่านทางเส้นเลือดดำ cubital หลังจากฉีดสารทึบรังสี 90 วินาที ทำการสแกนด้วยเอกซเรย์คอมพิวเตอร์สองพลังงานชนิดสลับค่าความต่างศักย์สูงสุดอย่างรวดเร็ว (80/140 เควีพี) และเอกซเรย์คอมพิวเตอร์พลังงานเดียว (120 เควีพี) ของช่องท้องทั้งหมด พารามิเตอร์การสแกนสำหรับเอกซเรย์คอมพิวเตอร์สองพลังงานมีดังนี้: ใช้การปรับกระแสหลอดเอกซเรย์แบบ GSI Assist; ความกว้างของคอลลิมเตอร์ 80 x 0.625 มม. ความเร็วในการหมุน 0.6 วินาทีต่อรอบ; พิทช์แฟกเตอร์ 0.992:1 พารามิเตอร์การสแกนสำหรับเอกซเรย์คอมพิวเตอร์พลังงานเดียวมีดังนี้: ความต่างศักย์ 120 เควีพี, ใช้การปรับค่ากระแสหลอดแบบอัตโนมัติด้วย 3D mA; เปิดคอลลิมเตอร์ 80 x 0.625 มม. ความเร็วในการหมุน 0.5 วินาที; พิทช์แฟกเตอร์ 0.992:1 ทำการประเมินปริมาณรังสีสำหรับทั้งสองโปรโตคอลในแง่ของดัชนีปริมาณรังสีในหุ่นจำลองเชิงปริมาตร(CTDI$_{vol}$) วิเคราะห์เชิงปริมาณโดยการวาด ROI ที่โครงสร้างช่องท้อง 5 ตำแหน่ง ได้แก่ หลอดเลือดแดงใหญ่, หลอดเลือดดำพอร์ทัล, ตับ, ม้าม และกล้ามเนื้อ psoas เพื่อประเมินค่าสัญญาณ (HU), ค่าสัญญาณรบกวน (SD), อัตราส่วนสัญญาณต่อสัญญาณรบกวน (SNR) และประเมินคุณภาพของภาพเชิงอัตนัยโดยรังสีแพทย์สองท่านที่มีความเชี่ยวชาญด้านภาพรังสีช่องท้อง โดยประเมินคุณภาพของภาพในแง่ของการยอมรับการวินิจฉัย (diagnostic acceptability) มี 4 ระดับและระดับของสัญญาณรบกวนภาพ (image noise) 3 ระดับ ตามเกณฑ์การประเมินคุณภาพของภาพเอกซเรย์คอมพิวเตอร์ของภาคพื้นยุโรป ผลการศึกษาพบว่าค่าเฉลี่ย CTDI$_{vol}$ สำหรับการตรวจเอกซเรย์คอมพิวเตอร์รังสีเอกซ์พลังงานเดียวมีค่าเท่ากับ 10.7±2.3 มิลลิเกรย์ และสำหรับการตรวจเอกซเรย์คอมพิวเตอร์รังสีเอกซ์สองพลังงานมีค่าเท่ากับ 10.3±2.8 มิลลิเกรย์ โดยไม่มีความแตกต่างอย่างมีนัยสำคัญทางสถิติระหว่างทั้งสองกลุ่ม (p>0.05) สำหรับการประเมินคุณลักษณะเชิงปริมาณ ผลที่ได้พบว่าค่าสัญญาณและค่าสัญญาณรบกวนมีค่าสูงขึ้นอย่างมีนัยสำคัญเมื่อใช้ตรวจเอกซเรย์คอมพิวเตอร์รังสีเอกซ์สองพลังงาน (p< 0.05) แต่ไม่มีความแตกต่างอย่างมีนัยสำคัญของอัตราส่วนสัญญาณต่อสัญญาณรบกวน ยกเว้นหลอดเลือดดำพอร์ทัล เมื่อเทียบกับเอกซเรย์คอมพิวเตอร์รังสีเอกซ์พลังงานเดียว สำหรับประเมินคุณภาพของภาพเชิงอัตนัย ผลที่ได้ไม่มีความแตกต่างกันอย่างมีนัยสำคัญระหว่างเอกซเรย์คอมพิวเตอร์รังสีเอกซ์พลังงานเดียวและสองพลังงานของการตรวจช่องท้องทั้งหมดในเรื่องการยอมรับการวินิจฉัยด้วยภาพเอกซเรย์คอมพิวเตอร์ระหว่างรังสีเอกซ์พลังงานเดียวและสองพลังงานและสัญญาณรบกวนภาพที่ถูกประเมินโดยรังสีแพทย์ทั้งสอง (p>0.05) โดยสรุปโปรโตคอลเอกซเรย์คอมพิวเตอร์สองพลังงานที่ใช้ในการศึกษานี้ให้คุณภาพของภาพเชิงปริมาณที่ใกล้เคียงกันและคุณภาพของภาพเชิงอัตวิสัยเทียบเท่ากับระดับปริมาณรังสีที่ใกล้เคียงกับเอกซเรย์คอมพิวเตอร์พลังงานเดียว ดังนั้นผลการศึกษานี้สามารถนำไปใช้เป็นโปรโตคอลประจำในห้องฉุกเฉินเพื่อลดปริมาณรังสีของผู้ป่วยในขณะที่รักษาคุณภาพของภาพและลดขั้นตอนการวินิจฉัยด้วยเอกซเรย์คอมพิวเตอร์สำหรับผู้ป่วยฉุกเฉินได้

สาขาวิชา	ฟิสิกส์การแพทย์	ลายมือชื่อนิสิต ....
ปีการศึกษา	2565	ลายมือชื่อ อ.ที่ปรึกษาหลัก ....

6470009130 : MAJOR MEDICAL PHYSICS
KEYWORD: Dual-energy CT, Single-energy CT, Volume CT Dose Index, Signal-to-noise ratio

Chanthawan Khemkhangboon : Comparison of radiation dose and image quality between fast kVp switching dual-energy CT and routine single-energy CT for whole abdomen at King Chulalongkorn Memorial Hospital. Advisor: Asst. Prof. KITIWAT KHAMWAN, Ph.D.

Abdominal computed tomography (CT) using a single energy protocol is a common imaging procedure in hospitals. As CT technology has continued to evolve, dual-energy protocols (DECT) have emerged as a new option. A spectral CT scanner with fast kVp switching was installed at King Chulalongkorn Memorial Hospital in 2017, and its clinical utility in emergency patients has not yet been studied. This study aims to compare the radiation dose and image quality between DECT and SECT in abdominal CT for emergency patients. The study retrospectively collected CT data from 130 standard-sized adult patients who underwent contrast-enhanced using the 256-slice MDCT. CT Contrast media was intravenously injected of iobitridol at a dose of 2.0 mL/kg with a flow rate of 2 mL/s through the median cubital vein. After the contrast medium was administered for 90 s, fast kVp-switching DECT (80/140 kVp,) and SECT (120 kVp) enhanced abdominal CT was performed. The scanning parameters for fast kVp-switching between 80 and 140-kVp were as follows: tube current, GSI Assist; detector collimation 80 x 0.625 mm; rotation speed 0.6 s; pitch factor 0.992:1. The scanning parameters for single-energy CT were as follows: 120 kVp, tube current 3D mA modulation; detector collimation 80 x 0.625 mm; rotation speed 0.5 s; pitch factor 0.992:1. The radiation dose was evaluated for both protocols in terms of $CTDI_{vol}$. Objective analysis was performed by measuring the region of interest (ROI) at 5 abdominal structures: aorta, main portal vein, liver, spleen, and psoas muscle in order to evaluate signal (HU), noise (SD), and signal-to-noise ratio (SNR). Subjective image quality was evaluated by two radiologists who have similar experience in terms of diagnostic acceptability on a 4-point scale and image noise on a 3-point scale following the European Guidelines on Quality Criteria. There was no statistically significant difference in average $CTDI_{vol}$ between SECT (10.7±2.3 mGy) and DECT (10.3±2.8 mGy) ($p>0.05$). The objective image quality analysis indicated that DECT had significantly higher signal and noise values compared to SECT for all measured structures ($p<0.05$), but there was no significant difference in SNR except MPV between the two groups ($p>0.05$). The subjective image quality analysis showed no significant difference in diagnostic acceptability and image noise between SECT and DECT as evaluated by both radiologists ($p>0.05$). In conclusion, the fast kV switching DECT protocol used in this study provides similar objective image quality and equivalent subjective image quality with a similar level of radiation dose as SECT. Therefore, the results of this study could be implemented as a routine protocol in the emergency room to reduce patient radiation dose while maintaining image quality and accelerating patient diagnostic workflow.

Field of Study:	Medical Physics	Student's Signature	
Academic Year:	2022	Advisor's Signature	

ACKNOWLEDGEMENTS

TABLE OF CONTENTS

จุฬาลงกรณ์มหาวิทยาลัย

CHULALONGKORN UNIVERSITY

LIST OF TABLES

LIST OF FIGURES

จุฬาลงกรณ์มหาวิทยาลัย
CHULALONGKORN **U**NIVERSITY

LIST OF ABBREVIATIONS

Abbreviation	Terms
AEC	Automatic Exposure Control
ASIR	Adaptive Statistical Iterative Reconstruction
CT	Computed Tomography
CTDI	Computed Tomography Dose Index
$CTDI_w$	Weighted Computed Tomography Dose Index
$CTDI_{vol}$	Volume Computed Tomography Dose Index
Cm	Centimeter
CNR	Contrast to Noise Ratio
DECT	Dual Energy Computed Tomography
DLP	Dose Length Product
DSCT	Dual Source Computed Tomography
FOV	Field Of View
HU	Hounsfield Unit
kVp	Kilo-Voltage Peak
keV	kiloelectronvolt
mm	Millimeter
mGy	Milligray
mGy.cm	Milligray centimeter
PMMA	Polymethylmethacrylate
PACS	Picture Archiving and Communication System
QC	Quality Control
ROI	Region Of Interest
SD	Standard Deviation
SECT	Single Energy Computed Tomography
Sn	Stannous - tin
SNR	Signal-to-Noise Ratio

CHAPTER I

INTRODUCTION

1.1 Background and Rationale

Computed tomography (CT) in medical imaging is growing due to its ability to represent the anatomy and pathology of internal organs for clinical diagnosis. However, materials of various compositions can be represented by the same or very similar CT numbers in CT imaging, making the differentiation and classification of different types of tissues extremely challenging. A simple example is the difficulty in distinguishing between calcified plaques and iodine-filled blood vessels. As a result, CT has been improved to be more efficient by employing dual energy CT (1), which can distinguish calcification from iodinated contrast media in blood vessels and soft tissue plaques from fatty tissue.

Dual-energy (DE) CT refers to a system that generates two photon spectra, characterized as attenuation measurements using separate energy spectra. The increased interest in DE scanning is being driven by three types of dual-energy CT scanners that differ in the technique used to acquire high- and low-energy CT datasets, e.g. a dual-source dual-energy scanner, a single-source dual-energy scanner with fast kilo-voltage switching (rapid alternation between high and low kilovoltage settings), and a single-source dual-energy scanner with dual detector layers (1).

DECT includes postprocessing applications that may be useful in abdominal and pelvic trauma, such as iodine selective imaging, virtual monenergetic imaging, and virtual noncalcium imaging. Iodine-selective imaging and virtual monoenergetic imaging can both improve the visibility of traumatic solid-organ and hollow visceral injuries, making them simpler to identify and classify. The use of iodine maps and virtual noncontrast pictures in iodine-selective imaging can aid in the assessment of active contrast extravasation. Virtual noncalcium imaging can reveal bone marrow edema, allowing for better identification of small fractures (2).

Computed tomography (CT) of the whole abdomen is one of the most common imaging performed in the hospital (3). CT is beneficial in various clinical cases in adults, including patients with non-specific abdominal pain, suspected appendicitis, abdominal trauma, and others. Every year, a large number of patients in Thailand are diagnosed with underlying abdominal injuries (2). These patients will be subjected to CT scans on many sessions in order to complete imaging exams promptly and properly. As a result, the patients will receive a higher cumulative radiation dose, which may contribute to a higher risk of future development (2).

Single-energy (SE) CT has some limitations in the evaluation of abdominal pathology. One of the main limitations is its lower contrast resolution compared to

DECT. SECT is less sensitive in detecting subtle differences in tissue attenuation, particularly in the presence of artifacts or image noise. This may lead to false-negative or false-positive findings, particularly in cases of small or low-contrast lesions. Another limitation of SECT is its inability to differentiate between iodinated contrast material and other materials with similar X-ray attenuation, such as hemorrhage, calcifications, or uric acid. This may limit its ability to detect active bleeding, particularly in cases of slow or intermittent bleeding, and may result in false-negative or false-positive findings.

The radiation doses and image quality characteristics of CT examinations are both regulated by the individual imaging procedure for each patient. The goal of each imaging technique is to provide visibility of anatomical structures and pathological signals while managing radiation exposure to achieve appropriate image quality. Although the scientific benefits of DECT have been demonstrated in multiple clinical scenarios, its routine clinical implementation has not been widespread, possibly due to concerns about increased radiation dose. In some clinical settings, DECT has been shown to be equivalent or superior to single-energy CT (SECT) in image quality and radiation dose (3). Therefore, it is of great interest in the radiation doses and image quality from DECT compared to single-energy routine protocol which can explore in determining the optimal imaging technique for this patient population.

1.2 Research objective

To compare the radiation dose and image quality between fast kVp switching dual-energy CT and routine single-energy CT for the whole abdomen at the emergency room at King Chulalongkorn Memorial Hospital.

1.3 Definitions

Dual-energy CT	The novel CT protocol technique, which consists of two CT datasets with distinct photon spectra, was developed by a number of suppliers with varying technological approaches. It can identify urinary stones and generating virtual non-contrast images from post-contrast enhanced scans.
Single-energy CT	The system that uses a single polychromatic X-ray beam (ranging from 70 to 140 kVp with a standard of 120 kVp) emitted from a single source and received by a single detector.
Volume CT Dose Index (CTDI$_{vol}$)	A measure used in computed tomography (CT) to quantify the radiation dose to the patient. It is defined as the average radiation dose delivered to a volume of tissue during a single rotation of the CT scanner, normalized to the nominal beam

width. The $CTDI_{vol}$ is typically reported in units of milligray(mGy).

Signal-to-noise ratio (SNR)   A quantitative measure used to describe the relationship between the signal (image information) and the background noise in the reconstructed image. It is defined as the ratio of the mean signal intensity within a region of interest (ROI) to the standard deviation of the background noise in the same ROI.

จุฬาลงกรณ์มหาวิทยาลัย
CHULALONGKORN UNIVERSITY

CHAPTER II

REVIEW OF RELATED LITERATURE

2.1 Theory

2.1.1 Computed Tomography (CT)

A computed tomography (CT) scan is a type of diagnostic imaging that employs x-rays to create cross-sectional images or slices of the body(1). Cross-sectional images are created by measuring the attenuation coefficient of the x-ray beam in the volume of the object. CT is founded on the fundamental concept that the attenuation coefficient may be used to calculate the density of the tissues crossed by the x-ray beam.

Early CT scanners only acquired images in slices (sequential scanning). However, since the 1980s, a continuously rotating x-ray tube and detector system, made by a slip-ring technology for electrical power supply and data acquisition, has been developed. This system uses a fan beam to cover the entire patient cross-section and corresponds to a detector array of scintillation detectors.

In 1989, Spiral or helical CT technique was developed, the mechanical moving the patient's table across the X-ray beam while the X-ray tube rotates continuously in one direction. As a result, the transmitted radiation appears a spiral or helix. It is possible to acquire information as a continuous volume of continuous slices rather than one slice at a time (Fig.2.1) (4). This minimizes the risk of artifacts brought on by patient movement by enabling greater anatomical parts of the body to be scanned during a single breath hold. A diagnostically meaningful scan is more likely to be obtained in patients who are unable to completely assist with the inquiry because to faster scanning, which also improves patient throughput.

Patient/table
movement

A
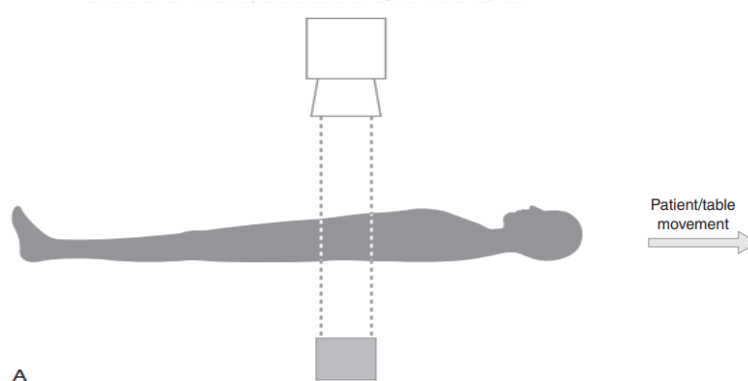
Figure 2.1 Single-slice system (One ring).

Now commercially accessible are CT scanners from the newest generation. The helical scanner's basic principles are utilized by these multislice or multidetector machines, which also have multiple rows of detector rings. By acquiring multiple slices every tube rotation, they can expand the region of the patient that the X-ray beam can cover in a given amount of time (Fig. 2.2) (4).
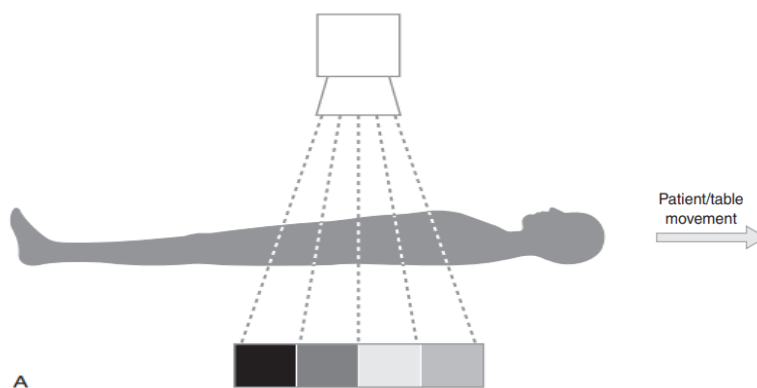
Figure 2.2 Multi-detector system.

2.1.2 Dual-energy CT

Dual energy CT, also known as DECT, generated two photon spectra; for this reason, DECT is also frequently referred to as spectral CT. The x-ray sources are made up of revolving anodes with polychromatic bremsstrahlung spectra that are overlaid with characteristic lines from the tungsten material of the anode. The voltage determines the maximum energy of the photons, although the mean energies are much lower, and their differences are smaller than one might anticipate. Because they offer the greatest difference and the least amount of overlap between the spectra with normal tubes, as shown in Figure. 2.3(4), the values of 80 and 140 kVp are frequently employed.
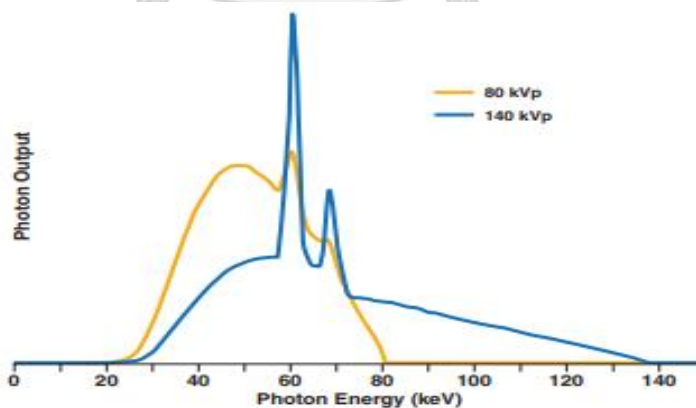
Figure 2.3 A 80 and 140 kVp combination for DECT systems. Both spectra's overlap is very wide.

Currently, there are three varieties that are commercially available.

2.1.2.1 Dual-Source CT(DSCT)

Dual-source CT is a system in which two x-ray sources and two associated detector systems are orthogonally arranged on the same gantry. Each x-ray tube works at a separate voltage, one lower and one higher, to produce the greatest disparity in their spectra. The latter has the least amount of spectral overlap. The tubes spin at a constant position relative to each other at the same time, preventing temporal discrepancies in projection sampling. Detector A has a diameter of 50 cm and covers the whole scan field-of-view, whereas detector B has a diameter of 26, 33, or 35 cm, depending on the exact scanner type(5), as illustrated in Figure. 2.4.
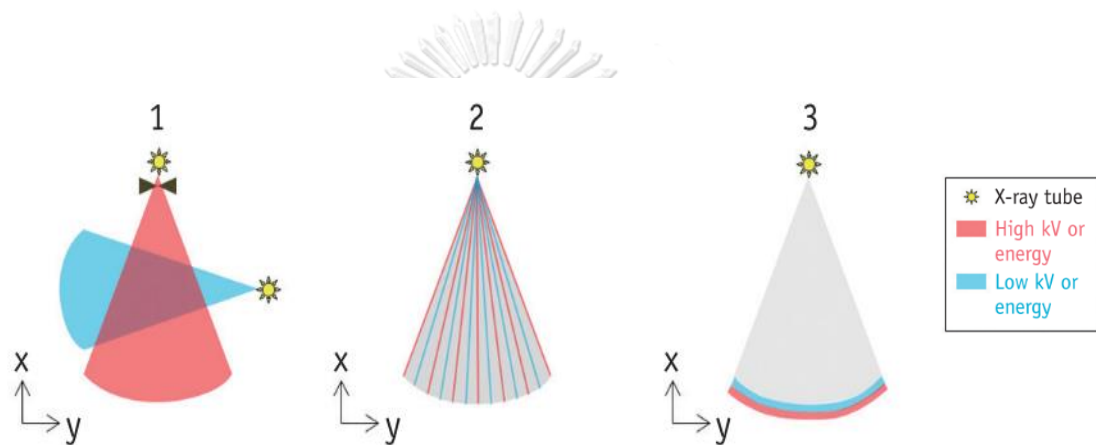
Figure 2. 4 Illustration of five different methods of dual-energy CT data acquisition. 1 = Dual-source CT,2 = rapid voltage switching with single tube, 3 = dual-layer detector with single tube.

2.1.2.2 Dual-Layer Detector

The dual-energy scan is performed at a single fixed-tube voltage, generally 120 kVp, unlike other methods using two different tube voltages. The inner thin layer consisting of yttrium-based scintillator absorbs low-energy photons selectively, while the outer thick layer of $Gd_2O_2S_2$ absorbs high-energy photons. The temporal difference between the dual-energy data is essentially non-existent. The projection-based technique utilized in the approach offers a potential benefit over image-based algorithms, notably in beam hardening correction, at the price of a greater noise level for material breakdown images (6). When compared to the image-based technique, the projection-based method often includes a laborious calibration procedure, a scatter issue, and intensive computing (6). Dual-energy evaluation may be conducted retrospectively following CT scanning in all clinical instances, which is a significant advantage in terms of workflow, but at the price of a somewhat long dual-energy reconstruction time. Dual-energy scanning is possible at full rotation speed (0.27 second) and full field of view (50 cm). However, because the sensitivity profiles of the scintillator materials between the two layers are significantly overlapped, the dual-

energy spectrum contrast is lower than that of dual tubes with beam filtering, as illustrated in Figure 2.4.

2.1.2.3 Fast kVp Switching.

Fast kVp Switching is a system in which the tube voltage is increased rapidly from 80 to 140 kVp, and the two projection data sets are separately recorded for use in a dual-energy reconstruction technique. The quality of two voltage-specific projection data is constrained by the rise and fall periods necessary for voltage modulation, therefore dual-energy CT scanning is only possible with a lowered gantry rotation speed (0.5 seconds or longer). As a result, the gantry rotation time must typically be at least 0.5 seconds, which increases the acquisition time. The slow gantry rotation significantly increases the motion artifacts, which cancels out the 0.5 ms. temporal difference between the two X-ray energy bands. Another significant issue with this approach is the difference in photon output between high and low voltages, which results in excessive radiation exposure to compensate up for the poor image quality. Recently, this problem was resolved by increasing the low-voltage exposure time ratio from 50 to 65%, however the dwell time ratio (65:35) cannot be further raised without worsening the angular mismatch between the two energy projections, as illustrated in Figure.2.4 (4, 5).

Moreover, the lower number of projections for each energy spectrum could result in a reduction in the overall image quality. The availability of tube current regulation for reducing radiation exposure and the limited dual-energy spectrum contrast are two additional drawbacks. The effectiveness of a projection-based algorithm in reducing beam-hardening artifact and providing accurate CT densitometry is not validated by this technique (7, 8). After dual-energy scanning, there are only 140 kVp images with high image noise that can be used for diagnostic imaging; this necessitates further reconstruction of virtual monoenergetic images, such as 70 keV imaging; despite a minor practical restriction in workflow, the image quality for diagnostic imaging is improved (Fig.2.5).

| A | B | C | D |
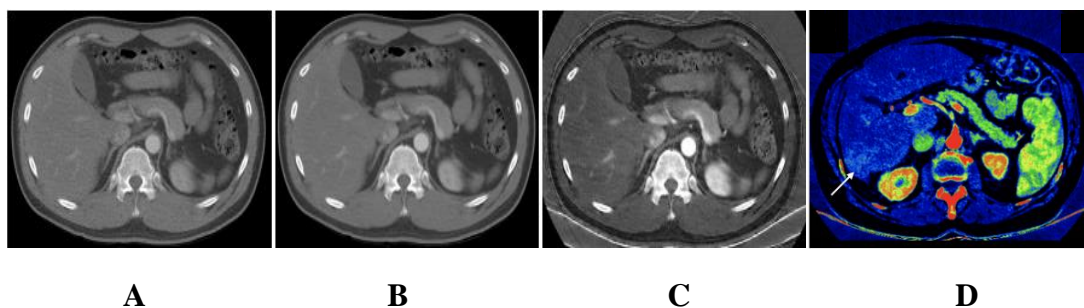
Figure 2.5 Abdominal CT images that have been contrast-enhanced utilizing rapid voltage switching system.

A. Image generated by using 140 kVp projections only shows high image noise.

B. Virtual monoenergetic image at 70 keV showing enhanced images must also be recreated for diagnostic imaging.

C. The improved iodine contrast-to-noise ratio is seen by the iodine map. Iodine maps show patient skin, clothing, and the CT table to be artificially bright.

D. Iodine color overlay on 55keV can better visualize recurrent cancer lesions (arrows).

2.1.3 Hounsfield unit or CT number

In CT images, the average of all the attenuation values found in the associated voxel is used to assign each pixel a numerical value (CT number)(9). Using a scale of arbitrary units called Hounsfield units (HU), this value is contrasted with the attenuation value of water as following in equation 2.1.

$$HU = \frac{\mu_{tissue} - \mu_{water}}{\mu_{water}} \times 1000 \qquad (2.1)$$

where μ_{tissue} is the average linear attenuation coefficient of tissue.

μ_{water} is the average linear attenuation coefficient of water.

An attenuation value (HU) of zero is used to calculate the CT number of water. Even though some contemporary scanners have a higher range of HU up to 4000, the wide range of CT numbers is 2000 HU. Each number corresponds to a different shade of the grey scale, with white (+1000) and black (-1000) at either end. Table. 1 displays each tissue's CT number.

Table 2.1 The Hounsfield unit in each tissue.

Tissue	CT number (HU)
Air	-1000
Lung	-200 to -500
Fat	-30 to -70
Water	0
Soft tissue	20 to 40
Bone	200 to 1000

2.1.4 Radiation dose

2.1.4.1. Computed Tomography Dose Index (CTDI)

The computed tomography dose index (CTDI) is the dosimetric quantity in CT (10). It can be measured free-in-air or in-phantom[2]. In most cases, a pencil ionization chamber is employed and CTDI is the average dose along the z axis from a sequence of continuous irradiations. The dosimetric quantities for both are known as CT kerma indices and are based on PKL measurements as shown in equation 2.2.

$$CTDI = \frac{1}{NT}\int_{-\infty}^{\infty} D(z)dz \tag{2.2}$$

where D(Z) is the dose profile along the z-axis.

N is the number of the detector rows of a single rotation.

T is the width of the tomographic section along the z-axis imaged by one data channel.

2.1.4.2. CTDI$_{100}$ (C$_{100}$)

The CTDI$_{100}$ is the quotient of the integral of the air kerma along a line parallel to the axis of rotation of a CT scanner over a length of 100 mm and the integration limits are 50 mm, which corresponds to the pencil ionization chamber's length of 100 mm. Measured free-in-air during a single rotation of a CT scanner as shown in equation 2.3(10).

$$CTDI = \frac{1}{NT}\int_{-50}^{50} D(z)dz \tag{2.3}$$

where D(Z) is the dose profile along the z-axis.

NT is nominal beam width.

2.1.4.3 Weighted CT Dose Index (CTDI$_w$, C$_w$)

The CTDI fluctuates throughout the field of vision (FOV) (10). For example, in body CT imaging, the CTDI is often a factor or two greater at the surface than in the middle of the FOV. The Weighted CTDI estimates the average CTDI over the FOV (CTDI$_w$) as shown in the equation 2.4.

$$CTDI_w = \frac{1}{3}CTDI100, center + \frac{2}{3}CTDI100, peripheral \tag{2.4}$$

Where CTDI$_{100, center}$ is radiation dose measured at the center of the phantom.

CTDI$_{100, peripheral}$ is the average value of radiation dose measured of all peripheral of the phantom.

2.1.4.4 Volume CT Dose Index (CTDI$_{vol}$, C$_{vol}$)

It is essential to account for any gaps or overlaps between the x-ray beams from successive rotations of the x-ray source in order to represent dose for a specific scan procedure, which nearly usually involves a series of scans. The Volume CTDIw (CTDI$_{vol}$) dose descriptor and milliGray as the SI unit are used to achieve this (mGy) (10). On the console of contemporary CT scanners, its value might be visible. CTDI$_{vol}$ is defined as:

$$CTDI_{vol} = \frac{N\times T}{I} + CTDI_w \tag{2.5}$$

Where I is the table increment per axial scan (mm)

$$\text{Pitch} = \frac{I}{(N \times T)} \qquad (2.6)$$

Since pitch is a ratio of the distance of the table move per rotation (I)

to nominal beam width (NT)

2.1.4.5 The factors that affect the radiation dose in CT.

2.1.4.5.1 Scan parameters

- Tube voltage (kilovolt: kV) represented by the peak energy of X-ray photons in the spectrum of X-ray energies (kilovoltage peak: kVp). While image contrast suffers when the tube potential is raised, the output of the tube and the beam's penetrating power both improve. For better tube loading and image quality in CT, higher tube voltages are preferred, and the connection between dose and tube potential is exponential in nature rather than linear, depending on the circumstances.

- Tube current-time product (milliampere-second: mAs) is a linear relationship between the tube current-time product and dose, meaning that all dose quantities will change by the same amount as the applied mAs. The number of photons produced, also known as radiation dose or radiation output, is proportional to mAs. Image noise results from variations in the tube current-time product and image quality.

- Rotation time is time to complete one 360° rotation of gantry. it results proportionate to the radiation dose, if quicker rotation times have lower dose all parameters kept constant. The need for full covering and halt motion might lessen the impact on the most affected.

- Pitch is a helical CT parameter that was introduced at the same time as the continuously moving table. Pitch is defined as the ratio of table feed per gantry rotation (cm) to x-ray beam z-axis width (cm). The radiation dose decreases proportionately as pitch is increased(11, 12).

2.1.5 Image quality

2.1.5.1 Image noise is a definition of the image signal's uncertainty.

The standard deviation in an image's uniform region of interest is used to measure image noise(11). Noise comes from a variety of places, including gain noise, electrical noise, structural noise, and quantum noise. It's depends on how many x-ray photons contributed to each detector measurement. However, the radiation dose to the patient increases as the number of photons increases.

2.1.5.2 Signal-to-noise ratio (SNR) is the signal over the entire item of

interest's dimensions.

The amount that this patch of the image is elevated in relation to the mean background signal is represented by the signal amplitude of each pixel. Since higher SNR makes it possible to notice tiny objects, images with higher SNR can enhance observer detection abilities as equation 2.7.

$$SNR = \frac{\bar{X}_s}{\sigma_{bg}} \qquad (2.7)$$

Where $\bar{X}_s$ is average value signal

σ_{bg} is noise or standard deviation value.

2.2 Review of related literature

Jeremy R, et al (3). assessed the radiation dose and image quality of routine dual energy CT (DECT) of the abdomen and pelvis performed in the emergency department setting and compared with single-energy CT (SECT). These representative CT datasets were collected from patients with routine contrast-enhanced SECT scans and dual-source DECT of the abdomen and pelvis meeting inclusion criteria matched by size and patient weight. Cohorts were compared in terms of radiation dose metrics of CT dose index (CTDI_vol) and dose length product (DLP) that recorded from the patient protocol screen capture report. Patient size was calculated using Equation (2.8) as followings:

$$Effective\ diameter = \sqrt{AP\ diameter\ x\ Lateral\ diameter} \qquad Equation\ (2.8)$$

For the equation, the effective diameter at the level of the main portal vein was calculated. Subjective measurement of image quality was evaluated by 2 experienced radiologists and objective measurements of image quality were measured in terms of signal, noise, and signal-to-noise ratio (SNR) of a variety of anatomical landmarks. To calculate noise, three standard deviation (SD) measurements were combined using Equation (2.9) as follows:

$$Noise = \frac{\sqrt{(a^2+b^2+c^2)}}{3} \qquad Equation\ (2.9)$$

where a, b, c defines three standard deviations (SD).

The signal to noise ratio (SNR) was calculated as the mean HU divided by the image noise (SD).

The scanning parameters to acquire the data are shown in Table 2.2.

Table 2.2 The comparison between SECT and DECT Protocols.

Parameters	SECT protocol	DECT protocol
Pitch	0.75	0.6
Rotation time(sec)	0.5	0.5
kVp	100,120, or 140	80/Sn140 or 100/Sn140
Reference mAs	275 (at 100 kVp)	400(80-kVp tube)
	180 (at 120 kVp)	201(100-kVp tube)
	133 (at 140 kVp)	155(140-kVp tube)
Kernel	I30f	I30f
Reconstruction	SAFIRE, level of 3	SAFIRE, level of 3
Contrast injection	Isovue370(weight-based protocol)	Isovue370(weight-based protocol)

They compared radiation dose as well as objective and subjective image quality for routine contrast enhanced DECT of the abdomen and pelvis with conventional single energy CT. DECT was performed with decreased radiation dose when compared with SECT, but demonstrated improved objective measurements of image quality, and equivalent subjective image quality. Both average $CTDI_{vol}$ and DLP were significantly lower in DECT than SECT. Average $CTDI_{vol}$ for SECT was 14.7 ($\pm$ 6.6) mGy and for DECT was 10.9 ($\pm$ 3.8) mGy, average DLP for SECT was 681.5 ($\pm$ 339.3) mGy.cm and for DECT was 534.8 mGy.cm respectively. The radiation dose for DECT was below the achievable doses found in a recent large study for contrast-enhanced abdominal CT. For objective image quality metrics, for all structures measured, noise was significantly lower, and SNR was significantly higher with DECT compared with SECT. In conclusion, their study proposed decreased radiation dose in DECT when compared to SECT, improved objective measurements of image quality, and equivalent subjective image quality.

Osman M, Basar S (13). reported 'Fast kilovoltage-switching dual-energy CT offering lower x-ray dose than single-energy CT for the chest: a quantitative and qualitative comparison study of the two methods of acquisition'. The objectives of this study were to compare the size-specific dose estimates (SSDE), CT dose indices and image quality parameters of the chest CTs obtained with fast kilovoltage-switching (FKS) dual-energy (DE) CT versus those with single-energy (SE) CT in chest SECT within the last 6 months. The 80/140 kVp on DECT and 120 kVp on SECT had been selected. Quantitative assessment in term of $CTDI_{vol}$, SSDE and contrast was defined as the difference of the mean HUs of the vascular bed and the cardiac spaces and the mean HU of the muscle. Image noise was defined as the mean SD of the subcutaneous fat tissue. Contrast-to-noise ratio (CNR) was defined as the ratio of the contrast to noise and Signal-to-noise ratio (SNR) was defined as the ratio of the mean HUs of the vascular bed and the cardiac spaces to the mean SD of them. Qualitative assessment in terms of image contrast, image noise, delineation of vessels within the mediastinum and the overall image quality assessed by two radiologists using interpreter scored. The results indicated that radiation dose and SSDE of FKS-DECT was lower with slightly higher image noise than SECT. In contrast, CNR of SECT was higher and SNR was lower than FKS-DECT respectively. Regarding vascular delineation and general image quality, SECT was higher than FKS-DECT. There was no significant difference in terms of other quantitative and qualitative image quality parameters.

Singh R, et al (14). reported the comparison of image quality and radiation doses between rapid kV-switching and dual-source DECT techniques in the patients underwent chest CT on both scanners 80/Sn150 kVp with automatic exposure control (AEC) in dual source CT (DS-DECT) and 80/140 kVp, noise index of 13–14 in single-source rapid kV switching CT (SS-DECT) had been set. Radiation dose was obtained from a commercial CT radiation dose tracking and monitoring software. Image quality was determined in terms of 60 keV virtual monoenergetic image (VMI) and decomposition- iodine (MDI) images. The results showed that at radiation doses and monoenergetic images from rapid kV-switching of the chest was 7.0±1.2 mGy and dual source CT was 8.4±1.2 mGy were similar, but there were considerable variations in appearance of material decomposition-iodine images acquired with these two techniques, when interpreting MDI images from SS-DECT due to artifactual heterogeneity in pulmonary perfusion. Artificial heterogeneity can obscure evaluation in patients with chronic pulmonary thromboembolic pulmonary hypertension who have subsegmental or atypical pulmonary perfusion defects on MDI images.

CHAPTER III

RESEARCH METHODOLOGY

3.1 Research design

This research is an observational descriptive designed in a type of retrospective study at a single center.

3.2 Research design model
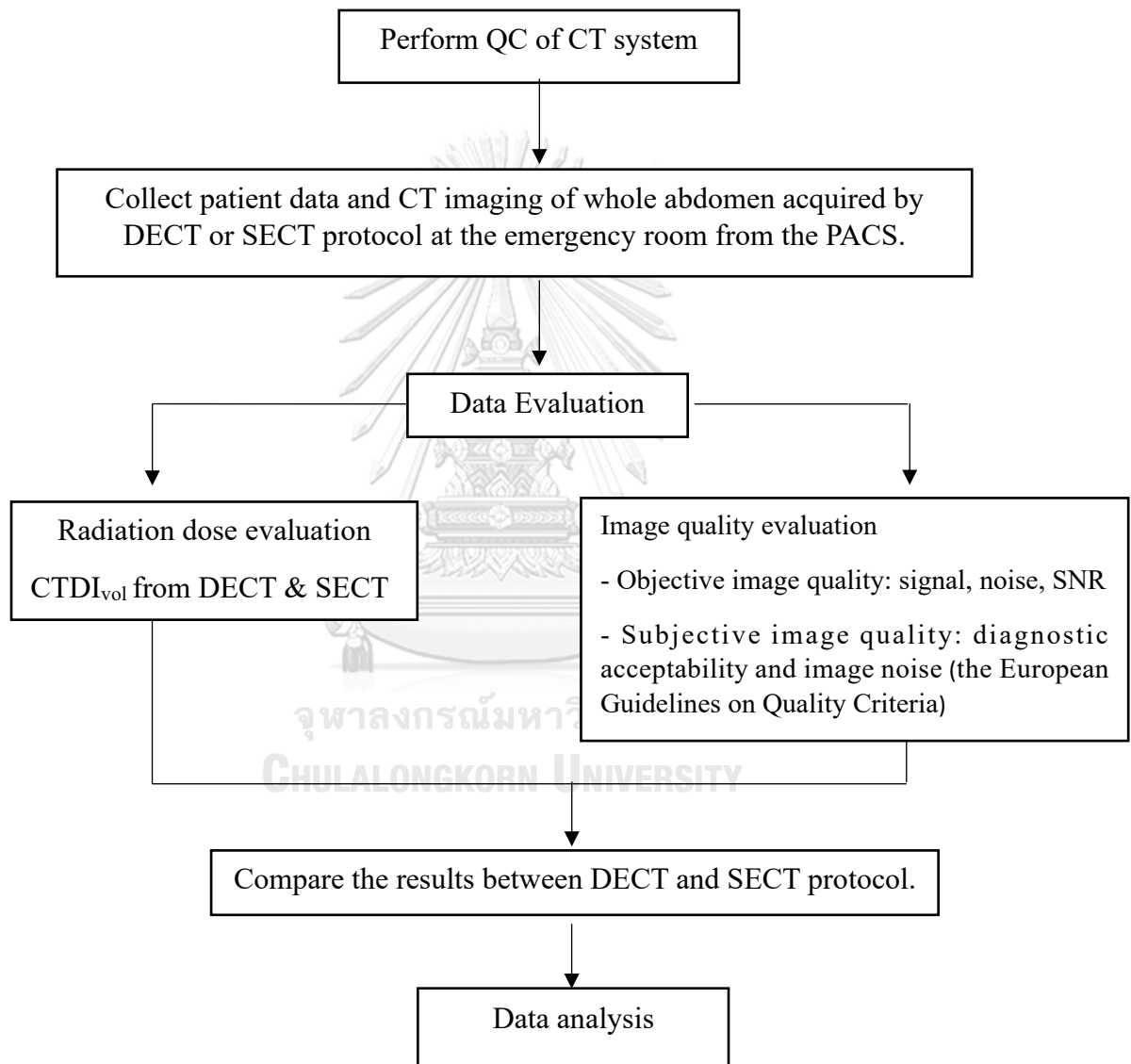
Figure 3.1 Research design model.

3.3 Conceptual framework

Image reconstruction

• Reconstruction filters

- Soft, Stnd, Detail

• Iterative reconstruction

- %ASIR

Data acquisition

- Tube current

- Tube voltage

- Pitch

- Rotation time(sec)

- Scan length

Performance characteristic of DECT&SECT

Patient demographic
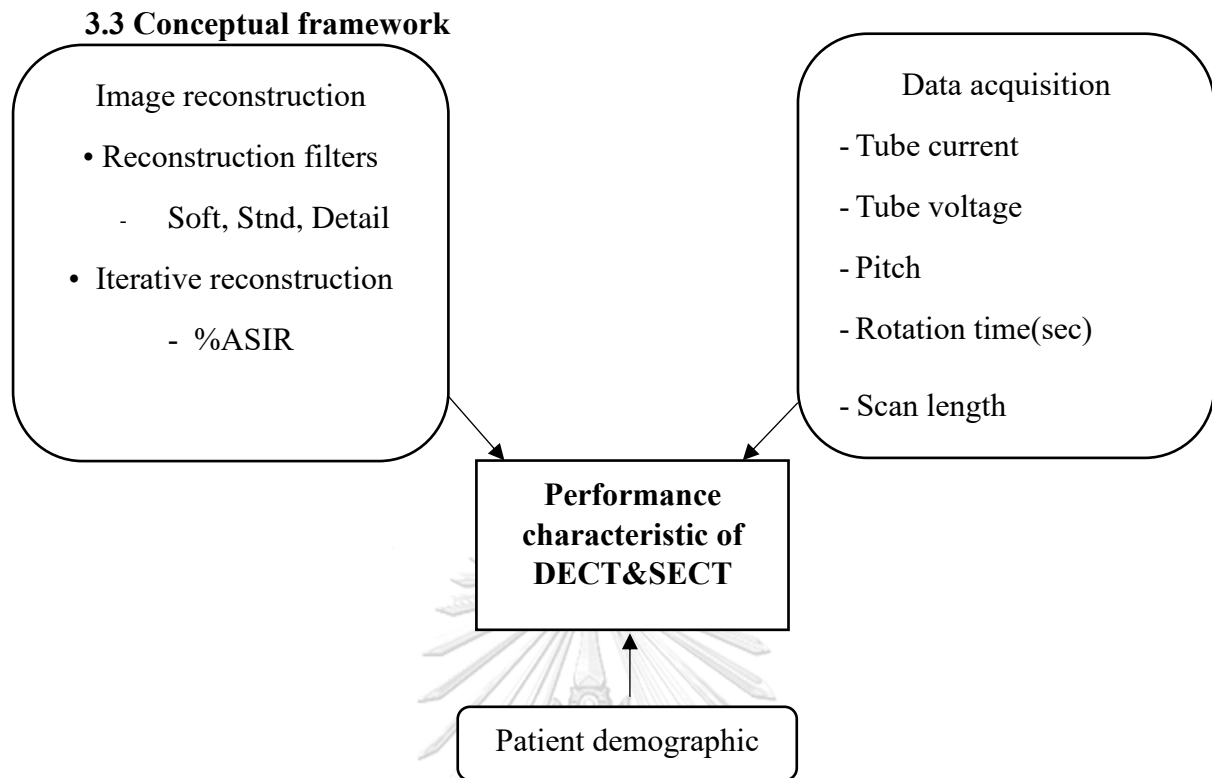
Figure 3.2 Conceptual framework.

3.4 Research question

What are the radiation dose and image quality of dual energy CT (DECT) using fast kVp switching and routine single-energy CT (SECT) in whole abdomen protocol performed at the emergency room at King Chulalongkorn Memorial Hospital?

3.5 Research objective

To compare the radiation dose and image quality between fast kVp switching dual-energy CT and routine single-energy CT for the whole abdomen at the emergency room, King Chulalongkorn Memorial Hospital.

3.6 Sample

3.6.1 Target population

The standard-sized adult patients who underwent portal venous phase CT of the whole abdomen between April 14, 2021 and April 30, 2023 at the emergency room at King Chulalongkorn Memorial Hospital.

3.6.2 Sample population

This study was a retrospective study. The patient demographics and CT scanning parameters were collected from Picture Archiving and Communication System (PACS).

3.7 Selection Criteria

    3.7.1 Inclusion criteria

      - Patient's age $\geq$ 15-yrs.

      - The patient's weight, with a standard size of 60±15 kg as suggested by the Ministry of Public Health's Department of Medical Sciences, and the patient's height (15).

      - Patients who underwent portal venous phase in the emergency room at King Chulalongkorn Memorial Hospital with either DECT or SECT protocol.

    3.7.2 Exclusion criteria

      - A patient who is younger than 15 years of age.

      - CT image series without $CTDI_{vol}$ dose report.

3.8 Sample size determination

The sample size was calculated using the following formula(3):

$$\frac{n}{gr} = \frac{2(Z_\alpha - Z_\beta)^2 \sigma^2}{(\mu_1 - \mu_2)^2}$$

Where: Z_α = 95% confidence interval = 1.96
Z_β = 80% Power = 0.84
μ_1 = Mean value sample size 1
μ_2 = Mean value sample size 2
σ^2 = Standard deviation (SD)

$$\frac{n}{gr} = \frac{2(1.96 + 0.84)^2(2.8)^2}{(14.6 - 10.9)^2}$$

$$\frac{n}{gr} = 33.22 \approx 33 \text{ patients per group}$$

3.9 Materials

    3.9.1 CT scanner

      The 256-slice CT scanner model GE Revolution fast kVp switching dual-energy CT was used in this study. The scanner has a single x-ray tube source capable of rapidly switching between low- and high-energy settings (80 and 140 kVp) and a single Gemstone Scintillator detector layer with 0.23 mm. High-definition imaging with the Gemstone™ Clarity Detector, full field of view of 50 cm, gantry rotation time up to 0.5 sec, table loading up to 306 kg, manufactured by General Electric (GE) Medical Systems, LLC (GE Healthcare) 3000 N. Grandview Blvd. Waukesha, WI, USA.(16) as shown in Figure 3.3. This scanner is a new generation of fast kV switching during dual-energy CT, with variable (GSI Assist) to modulate the tube

current. The system was installed at the 1st floor of the emergency room, King Chulalongkorn Memorial Hospital on 24th October 2017.

Figure 3.3 256-Slice GE Revolution CT at Emergency Room, KCMH.

3.9.2. Picture Archive and Communication System (PACS)

Picture archiving and communication system (PACS) is an information technology system that aids in picture transmission from the point of image collection to various physically dissimilar locations. This technology is not only cost effective (film-free department), but also allows for simultaneous access to numerous modalities (radiographs, CT, MR, ultrasound, etc.) at multiple locations inside hospitals or around the world. In this investigation, the Synapse PACS system was utilized to extract axial images for data analysis, measurements, and radiation dose reporting.

Figure 3.4 Picture Archive and Communication System (PACS).

3.9.3 PMMA phantom

Polymethylmethacrylate was used to create two cylindrical CT phantoms. They are intended for dosimetric measurement of head and body CT protocols with diameters of 16 cm, 32 cm, respectively. Both phantoms have five holes, one in the center and four on the edges, all located one centimeter from the phantom edge. For the purpose of using acrylic rods and a pencil ion chamber for all holes during the radiation dose measurement, all holes were inserted (17) as shown in Figure. 10.
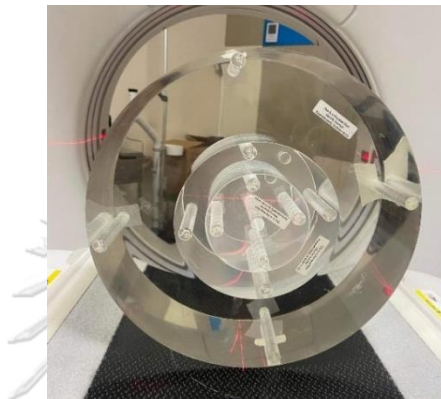
Figure 3.5 PMMA phantoms of 16, 32 cm in diameter and acrylic rods

3.9.4 CATPHAN® 600 phantom

Catphan® 600 phantom was employed for CT scanner performance as part of the image quality evaluation. At the end of the box, where it is placed on the CT table, the CATPHAN® phantom is suspended in midair. By carefully indexing the table from the center of section 1 (CTP404) to the center of each succeeding test module, all test sections may be found. The following is a list of the indexing distances from the first section (18):

Module	Distance from section 1 center
CTP404, Slice width sensitometry and pixel size	0 mm.
CTP591, Bead geometry	32.5 mm.
CTP528, 21line pair high resolution	70 mm.
CTP528, Point source	80 mm.
CTP515, Sub-slice and supra-slice low contrast	110 mm.
CTP486, Solid image uniformity module	150 mm.
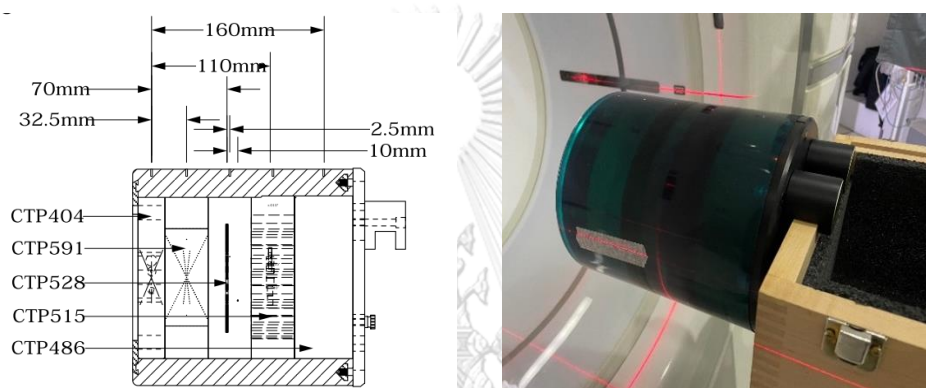
Figure 3. 6 Catphan® 600 phantom.

3.9.5 The pencil type ionization chamber and dosimeter

Figure 3.7 The ionization chamber for measurement of Computed Tomography Dose Index (CTDI)

Figure 3.7 shows a CT pencil ionization chamber with a 3 cm^3 active volume and a 10 cm active length. It is created for CT x-ray beam measurements, either free-in-air or installed in a head or body phantom. One property of this chamber is its consistent reaction to incoming radiation at all angles around its axis. The pencil ionization chamber model Radcal 10X6-3CT, and Accu-Gold dosimeter (Figure 3.8).were utilized for measuring the radiation dose, and recording the dosimetric amount in this investigation (19, 20).

Figure 3.8 Radcal® Accu-Gold+ digitizer module.

3.10 Methods

3.10.1 The performance of CT had been evaluated according to the IAEA

Human Health no.19 and CATPHAN® 600 manual.

The program consists of:

- Mechanical accuracy

- Dosimetry CTDI in air and CTDI in phantom

- Image quality performance

3.10.2 Collect patient data

The information was gathered from patients who underwent portal venous phase of the whole abdomen CT at emergency room, King Chulalongkorn Memorial Hospital and had a standard body weight of 60±15 kg, as well as their height, gender, and age. The number of patients gathered was 50 per protocol.

Patient data were collected from patients who had undergone a portal venous phase whole abdomen CT at the emergency room of King Chulalongkorn Memorial Hospital and had a standard body weight of 60±15 kg, align with their height, age, and gender. Each protocol included at least 50 patients.

3.10.3 CT scan protocol

All patients who underwent whole-abdominal CT with either DECT or SECT acquired by 256-slice GE Revolution CT scanner at emergency room, King Chulalongkorn Memorial Hospital with a standardized protocol were scanned using the following parameters:

Table 3.1 Imaging parameters for DE and SECT protocols

Parameter	DECT	SECT
Tube voltage (kVp)	80/140	120
Noise index (HU)	10	10
Tube current (mA)	Variable (GSI Assist)	3D mA modulation
Beam collimation (mm)	80 x 0.625mm	80 x 0.625mm
Rotation time (s)	0.6	0.5
Pitch	0.992:1	0.992:1
Scan field of view (cm)	50	50
Image reconstruction	ASiR-V 40%	ASiR-V 40%
Contrast injection	Xenetix 300 (100ml)	Xenetix 300 (100ml)

3.10.4 Objective image quality evaluation

3.10.4.1 All image analysis was performed on PACS. Performance characteristics in terms of quantitative image quality were evaluated by signal (HU), signal-to-noise ratio (SNR), and image noise (SD).

3.10.4.2 The signals (HU) & image noises (SD) were measured from 70 keV VMI transaxial images in DECT protocol and transaxial venous phase in SECT protocol in each patient.

3.10.4.3 These parameters were measured by placing round ROIs of 25-150 mm^2 within the aorta, and main portal vein (MPV), whereas ROI sizes of 200–300 mm^2 were measured within liver, spleen, and psoas muscle on image as shown in Figure 3.9.

A   **B**
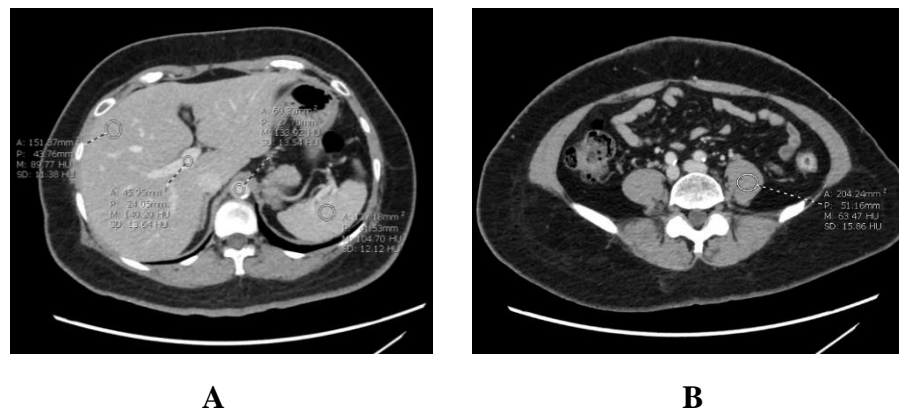
Figure 3.9 The measurement of signal and image noise in each anatomical structure of liver, MPV, aorta, spleen (A) and psoas muscle (B).

3.10.4.4 The signal of each anatomical structure was measured, and the average CT number was calculated.

3.10.4.5 The signal of each anatomical was measured in ROI with a similar area of each structure. The noise of each anatomical was determined by the standard deviation (SD).

3.10.4.6 The SNR was calculated as the ratio between the CT number of each anatomical structure and noise using equation 3.1 as followings:

$$SNR = \frac{CT\ No_{ROI}}{SD_{ROI}} \qquad (3.1)$$

where CT No.$_{ROI}$ is mean CT number in each anatomical structure, SD$_{ROI}$ is the standard deviation in each anatomical structure.

3.10.5 Subjective image quality evaluation

- Subjective image quality was scored independently by two radiologists who have the of experience in abdominal CT imaging at least 5 years.

- The radiologists evaluated the images for diagnostic acceptability and image noise using a 4-point scale, and a 3-point scale respectively according to the European Guidelines on Quality Criteria (18), as shown in Table 3.2. A grading of lower than or equal to 2 was considered poor for diagnostic acceptability and grading of greater than 2 was considered excessive noise.

- The average scoring of image noise and diagnostic acceptability were compared between DECT and SECT protocol graded by each radiologist.

Table 3.2 The European Guidelines on image quality criteria for subjective image quality assessment.

Rating	Subjective analysis of image noise (SAN)	Diagnostic acceptability (DA)
1	Too little noise	Unacceptable
2	Acceptable noise	Acceptable only under limited conditions for visualization of abnormalities
3	Excessive noise	Acceptable for interpretation
4		Fully acceptable for diagnostic interpretation

3.10.6 Radiation dose

The radiation doses obtained from each protocol were evaluated in terms of CTDI$_{vol}$, which was recorded from the PACS system.

3.11 Data analysis

The radiation doses in terms of CTDI$_{vol}$, the subjective and objective image quality, image noise and SNR, obtained from both DECT and SECT were determined by using Microsoft excel software to obtain the maximum, minimum, mean, standard deviation values.

3.12 Statistical Analysis

Descriptive statistic parameters in this research were: maximum, minimum, mean and standard deviation (SD) by using Microsoft excel software and SPSS V19.0 (IBM, Armonk, New York).

3.13 Outcome measurement

- Average CTDI$_{vol}$ derived from DECT and SECT protocols.
- Image quality in terms of signal, noise and SNR obtained from whole-abdominal CT DECT and SECT protocol in emergency patients.

- Results of subjective image quality scoring by radiologists.

3.14 Expected Benefits

To obtain the radiation dose and image quality evaluation acquired by fast kVp switching dual-energy CT and routine single-energy CT for whole-abdominal in emergency room at KCMH.

3.15 Ethical consideration

This study was conducted in accordance with the guidelines set forth by the Institutional Review Board (IRB) of the Faculty of Medicine, Chulalongkorn University, Bangkok, Thailand (IRB NO. 0415/65), which approved the research proposal after evaluating its compliance with ethical considerations to retrospectively collect the patient demographics, CT scanning parameters, and related values from PACS system.

CHAPTER IV
RESULTS

4.1 Quality control of CT scanners

CT scanner quality control was carried out in accordance with IAEA Human Health Series no.19 and IAEA TRS no.457 in terms of the electromechanical system, image quality, and radiation dose verification. The details of the results and reports are shown in the appendix B. The summarized reports of CT system performance test are illustrated in Table 4.1.

Table 4.1 Report of CT system performance.

Location: Bhumisiri Building (1st floor) King Chulalongkorn Memorial Hospital
Date: 18 February 2023
Manufacture: GE Healthcare
M/N and S/N: Revolution CT

RESULTS	LISTS OF QUALITY CONTROL
Pass	Alignment of Table to Gantry
Pass	Scan Localization Light Accuracy
Pass	Table Increment Accuracy
Pass	C.T.# Position Dependence and S/N
Pass	Reproducibility of C.T. Numbers
Pass	mAs Linearity
Pass	Linearity of C.T. Numbers
Pass	High Contrast Resolution
Pass	Low Contrast Resolution
Pass	Slice Thickness Accuracy
Pass	Image Uniformity
Pass	Accuracy of Distance Measurement
Pass	CTDI Verification

4.2 The patient data collection

The patient data were collected from 130 cases of whole abdomen with DECT and SECT protocols during April $14, 2021$ and April $30, 2023$ from the Radiology Department and the Emergency Department at the King Memorial Chulalongkorn Hospital (KCMH). The patient's standard size was recommended by the Department of Medical Sciences, Ministry of Public Health for 60±15 kg body weight. The patient demographic data of gender, age, weight, BMI, and height are shown as in Table 4.2. It was found that there were no statistically significant differences between SECT and DECT with respect to patient selection and patient data analyzed in this study. Therefore, the two imaging techniques are comparable in terms of these mentioned factors.

Table 4.2 Patient data on gender, age, weight, BMI, and height of DECT and SECT protocols.

Patient data	SECT	DECT	p-value
Gender (M/F)	27 / 38	23 / 42	>0.999
Age (yr)	59.9 ± 17.8 (16 − 88)	55.4 ± 18.3 (19 − 93)	0.168
Weight (kg)	59.2 ± 8.0 (45 - 75)	58.3 ± 7.9 (45 - 75)	0.514
Height (cm)	162.4 ± 7.3 (150 - 185)	162.1 ± 7.2 (147 - 182)	0.838
BMI (kg/m^2)	22.5 ± 2.9 (17 -29)	22.2 ± 2.9 (16 - 29)	0.535

4.3 Image acquisition

The examples of portal venous phase images obtained from DECT and SECT protocols in the study are shown in Figures 4.1 and 4.2, respectively. All images were displayed at a slice thickness of 2.5 mm.
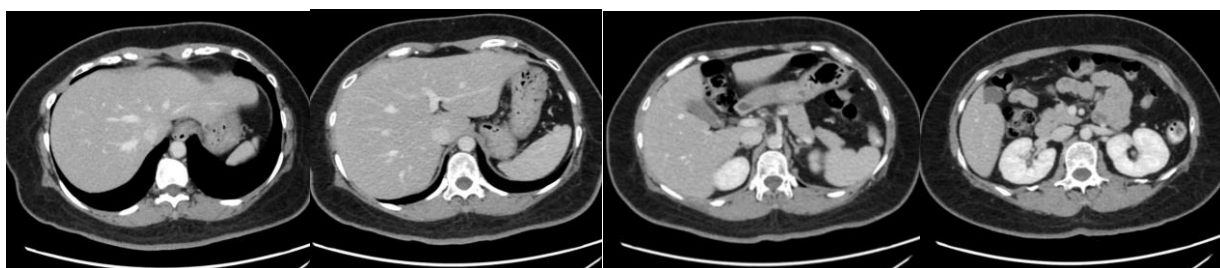
Figure 4.1 The portal venous phase image quality obtained from SECT.
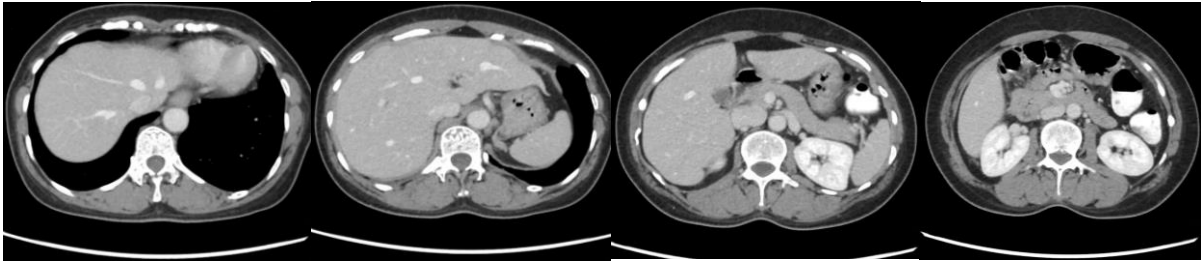
Figure 4.2 The portal venous phase image quality obtained from DECT using VMI at 70 keV.

4.4 Objective image quality evaluation

4.4.1 Signal (HU)

In order to evaluate the quantitative image quality, the signal in terms of CT HU was measured at the aorta, MPV, liver, spleen, and psoas muscle of single- and dual-energy composition images as shown in Table 4.3 and figure 4.3.

Table 4.3 The average HU obtained from each organ of the portal venous phase from DECT and SECT protocols.

Region	SECT	DECT	%Diff.	p-value
Aorta	154.3 ± 17.8 (118 - 191)	178.8 ± 27.8 (122 - 258)	15.9	$< .00001$
MPV	159.3 ± 19.1 (118 – 202)	187.4 ± 28.1 (126 - 253)	17.6	$< .00001$
Liver	113.8 ± 10.4 (89 – 135)	122.4 ± 16.7 (89 - 157)	7.5	0.001
Spleen	122.6 ± 12.8 (97 – 173)	131.7 ± 17.0 (97 - 185)	7.4	0.001
Psoas muscle	59.7 ± 5.9 (44 – 72)	62.8 ± 6.2 (46 - 74)	4.2	0.014

$\%\text{Difference} = \frac{|HU_{DECT} - HU_{SECT}|}{HU_{SECT}} \times 100$

Box plot of signal from DE & SECT protocol for each organ in the portal venous phase image
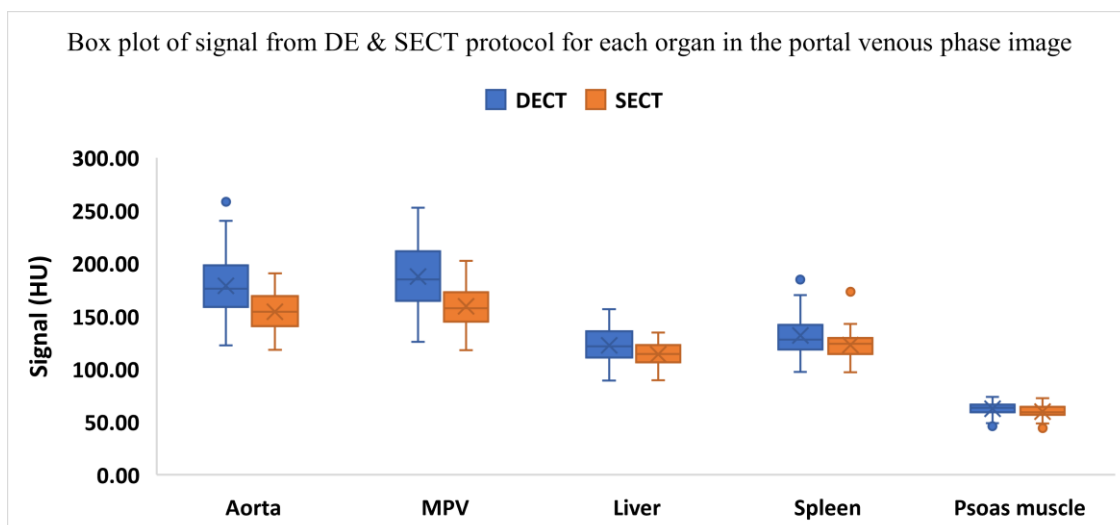
Figure 4.3 Box plot of HU measured from DE & SECT protocols for each organ in the portal venous phase.

From Table 4.3, it was found that the average CT number of DECT images was higher than SECT in all organs, including the aorta, MPV, liver, spleen, and psoas muscle. The MPV had the highest %difference of 17.6, which was considered the highest value. However, all values were within normal range, and the CT number values measured from Figures 4.3 showed that the distribution of CT values in DECT was higher than SECT and had a statistically significant difference ($p<0.05$).

4.4.2 Image noise (SD)

The image noise was obtained from the standard deviation of CT number measurement, by drawing an ROI at the aorta, MPV, liver, spleen, and psoas muscle on image of single- and dual-energy composition images. The image noises in terms of SD results are shown in Table 4.4.

Table 4.4 The results of SD measured in each organ of DECT and SECT protocols in portal venous phase.

Region	SECT	DECT	%Diff.	p-value
Aorta	12.9 ± 1.8 (7 - 18)	14.1 ± 2.0 (10 - 19)	9.6	< 0.00001
MPV	12.5 ± 1.4 (10 - 17)	13.8 ± 2.3 (9 - 24)	10.5	< 0.00001
Liver	11.7 ± 1.1 (9 - 14)	12.7 ± 1.6 (9 - 18)	9.3	< 0.00001
Spleen	12.3 ± 1.5 (8 - 16)	13.3 ± 2.0 (9 - 19)	8.5	0.001
Psoas muscle	13.2 ± 1.2 (10 - 20)	14.2 ± 1.6 (10 - 18)	7.5	0.001

$$\%\text{Difference} = \frac{|\,SD_{DECT} - SD_{SECT}\,|}{SD_{SECT}}\,\text{x}100$$
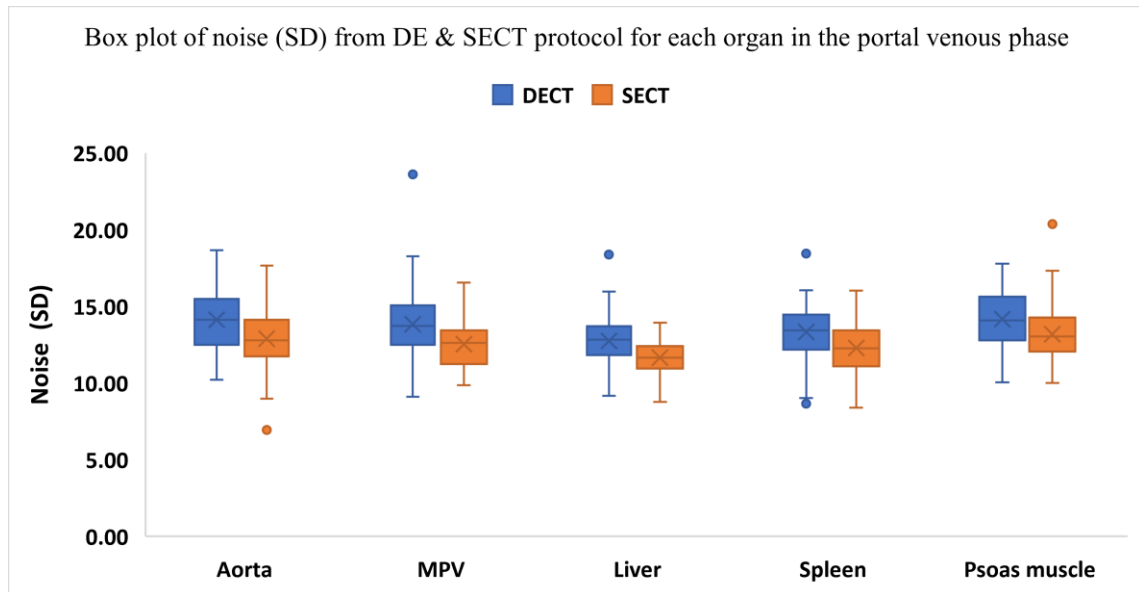
Figure 4.4 Box plot of noise (SD) from DE & SECT protocol for each organ in the portal venous phase.

From Table 4.4. The average value of noise for all organs was found to be higher in DECT than SECT protocol, while the MPV had %difference of 10.5, which is consistent with the signal values from the graph as mentioned previously. The distribution characteristics of noise for DECT was higher than SECT and had a statistically significant difference ($p < 0.05$), as shown in figures 4.4.

4.4.3 Signal to Noise Ratio (SNR)

SNR was calculated as the mean HU divided by the image noise in each organ for comparison of single- and dual-energy composition images as shown in Table.4.5.

Table 4.5 SNR of single- and dual-energy protocols in portal venous phase.

Region	SECT	DECT	%Diff.	p-value
Aorta	12.2 ± 2.2 (8 - 21)	12.9 ± 2.7 (9 - 19)	5.8	0.104
MPV	12.9 ± 2.0 (9 - 20)	13.9 ± 2.8 (7 - 23)	7.7	0.022
Liver	9.9 ± 1.4 (7 - 14)	9.8 ± 1.9 (5 - 17)	1.0	0.736
Spleen	10.1 ± 1.6 (7 ± 16)	10 ± 1.6 (7 - 13)	0.8	0.777
Psoas muscle	4.6 ± 0.8 (3 - 6)	4.5 ± 0.8 (3 - 7)	3.1	0.242

$$\%\text{Difference} = \frac{|\,SNR_{DECT} - SNR_{SECT}\,|}{SNR_{SECT}}\,\text{x}100$$

Box plot of SNR from DE&SECT protocol for each organ in the portal venous phase.
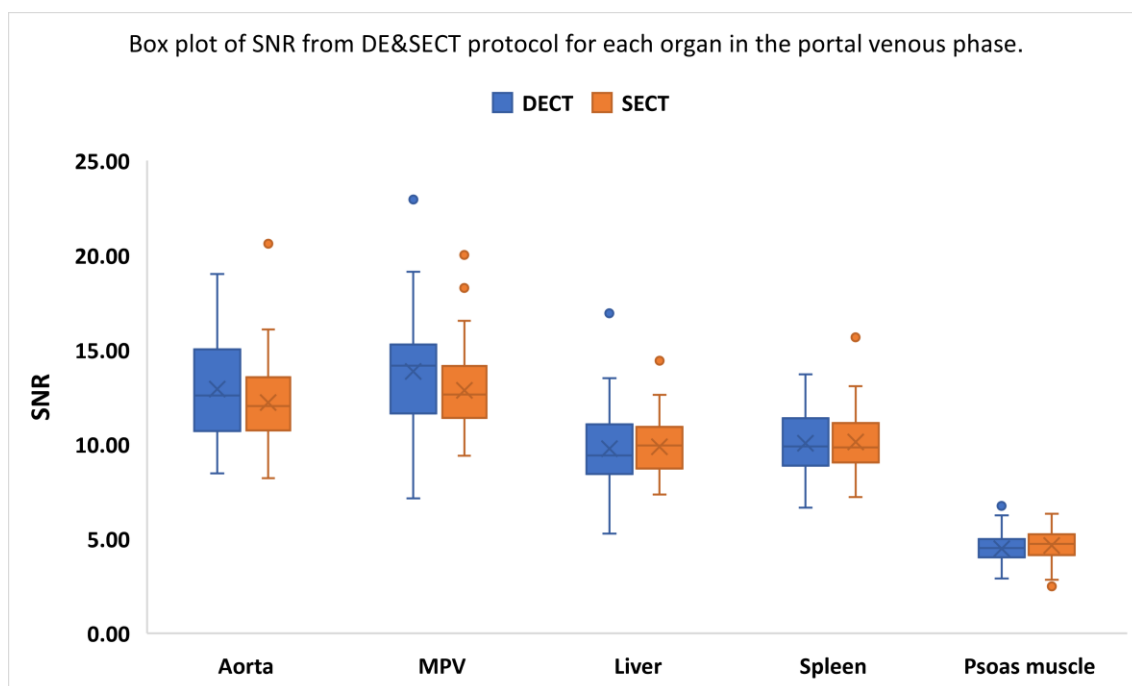
Figure 4.5 Box plot of SNR from SECT protocol for each organ in the portal venous phase.

Table 4.5 shows that the SNR values obtained from DECT protocol were comparable to those from SECT in the liver, aorta, and psoas muscle, except for the spleen with the same SNR values as compared to other organs. Figure 4.5 demonstrates the distribution of SNR data, revealing a similar distribution pattern for both DECT and SECT protocols with only minor differences.

4.5 Subjective image quality evaluation

- The Observers

The images of each acquisition protocol were reviewed by two radiologists who have a similar experience for the DECT in abdominal CT examination such that they were blinded the parameter settings. Subjective image quality grading was performed on the axial 2.5/1 mm images sent to PACS for routine interpretation. The CT scanning images were graded in random order and were displayed in standard window/level settings, which could then be freely adjusted by the reader.

- Image quality scores for DE & SECT protocols.

Table 4.6 Diagnostic acceptability scores for DE & SECT protocols in portal venous phase.

	Diagnostic acceptability		p-value
	DECT (70 keV)	SECT (120 kVp)	
Radiologist 1	3.9 ± 0.2	3.9 ± 0.2	>0.999
Radiologist 2	3.9 ± 0.3	4.0 ± 0.1	0.865
Kappa value	0.919		

Table 4.7 Subjective analysis of image noise scores for DE & SECT protocols in portal venous phase.

	Subjective analysis of image noise		p-value
	DECT (70 keV)	SECT (120 kVp)	
Radiology 1	2.0 ± 0.0	2.1 ± 0.2	0.549
Radiology 2	2.0 ± 0.0	2.0 ± 0.2	0.764
Kappa	0.660		

Table. 4.6 and 4.7, show the summarized results on image quality evaluation for image noise and diagnostic acceptability in the DECT and SECT. The image noise (p =0.549 for radiologist 1, p =0.764 for radiologist 2) and diagnostic acceptability (p > 0.99 for radiologist 1 and p = 0.865 for radiologist 2) were slightly lower in the DECT group than in the SECT group. No difference was observed in diagnostic acceptability between the two groups interpreted by radiologist 1 (p>0.999). The *k-values* ranged from 0.660 to 0.919, indicating a substantial, and almost perfect agreements between the two readers. The number of cases with equal to three points (diagnostic) in diagnostic acceptability were 3 (4.6%) in SECT, 3 (4.6%) in DECT and image noise with greater two points were 4 (6.2%) in SECT and 0 (0%) in DECT for readers 1 and 3 (4.6%) in SECT, 4 (6.2%) in DECT and image noise were 2 (3.1%) in SECT, 0 (0%) in DECT for readers 2, respectively.

4.6 Radiation dose

Average $CTDI_{vol}$ was recorded at 70 keV VMI portal venous phase in DECT and 120 kVp portal venous phase in SECT protocol from PACS with parameter settings are shown in Table 4.8.

Table 4.8 Comparison of radiation dose between DECT and SECT in portal venous phase.

CTDI$_{vol}$	SECT (120 kVp)	DECT (70 keV)	*P-value*
	10.7 ± 2.3	10.3 ± 2.8	0.406
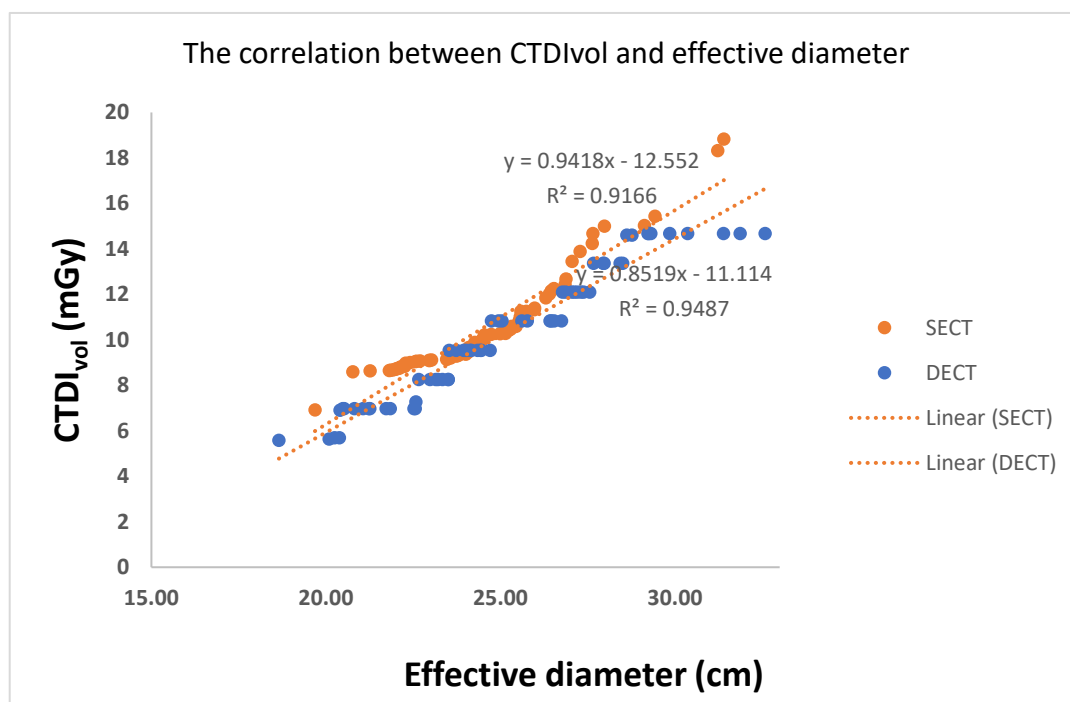
Figure 4.6 The correlation between CTDI$_{vol}$ and effective diameter.

Table 4.8 demonstrates that the average CTDI$_{vol}$ for SECT was 10.1±2.3 mGy, and for DECT was 10.3±2.8 mGy. There were no significant differences between both of DECT and SECT (p=0.406) for the average scans CTDI$_{vol}$ values. The average CTDI$_{vol}$ in the DECT group was 3% lower than those in the SECT group. A strong correlation was found between CTDI$_{vol}$ and patient size for SECT and DECT with R^2 of 0.9166 and 0.9487, respectively, as shown in Fig 4.6.

CHAPTER V

DISCUSSION AND CONCLUSIONS

5.1 Discussion

In this study, patient data from patients who underwent venous phase of the whole abdomen with DECT and SECT protocols were collected. The performance characteristics were evaluated in the aspects of objective image quality in terms of signal, image noise and SNR, and subjective image quality evaluated by two radiologists, and the radiation dose aspect in terms of $CTDI_{vol}$ value between DECT and SECT protocol in clinical settings in emergency room at King Chulalongkorn Memorial Hospital.

5.1.1 Signal (HU), noise (SD) and signal-to-noise ratio (SNR)

The average signal and noise of all anatomical sites were significantly higher in the DECT group than in the SECT group ($p > 0.05$). This phenomenon may be attributed to the limitations associated with using a longer tube rotation time of rapid fast-switching kVp for DECT compared to SECT, which typically takes 0.5 seconds or more. This finding is consistent with previous studies by Goo HW, et al (5) and Noda Y, et al (21) . To address this, the low-voltage exposure time ratio was increased from 50 to 65%, resulting in predominant an accentuated CT number near the iodine k-edge. This led to elevations of the CT numbers of organs and vessels as well as background noise on contrast-enhanced DECT images. In addition, rapid fast-switching kVp for DECT, the tube alternates rapidly between the two tube potentials (80 and 140 kVp) during the same rotation time, but the tube current cannot be changed simultaneously, which results also higher noise on DECT images obtained with lower peak voltage (22).

Nevertheless, the SNRs of MPV in the DECT group were superior to the SECT group, which is consistent with the study of Noda Y et al (23, 24). The major cause was the existence or absence of an automated tube current modulation scheme. Based on a prior study, SECT can be adjusted the tube current automatically based on the participant's body size to optimize the radiation dose while maintaining image noise. In contrast, DECT did not automate tube current modulation. This might degrade the imaging quality, particularly in the pelvic area. This study, the SNRs of all anatomical structure in 70 keV were similar to those acquired by SECT 120 kVp. Several studies also suggested that the energy levels between 60–70 keV can provide an optimal trade-off between contrast enhancement and acceptable noise for routine DECT (7, 25, 26) .

5.1.2 Subjective image quality

The image quality for image noise and diagnostic acceptability in the DECT and SECT groups are summarized in Table 4.6 and 4.7. No statistical difference was observed in image quality between the two groups. However, the number of cases with ≤ 3 points (diagnostic) in diagnostic acceptability were totally 7/130 (5.3%), > 2 points

in image noise were totally 4/130 (3.1%) between both groups. All cases with lower scores were due to the presence of metallic artifacts from hip prostheses, which were not a result of using SECT or DECT protocol as shown in Figure 5.1. The measurements of these parameters exhibited a notable agreement between the two radiologists. For instance, among the 65 SECT cases, the first radiologist identified 4 (6.2%) with excessive noise in image quality, while none of the 65 DECT cases were flagged. Similarly, the second radiologist identified 2 (3.1%) SECT cases with excessive noise out of the 65 examined, with no instances found among the 65 DECT cases. The subjective nature of image quality measurements in this study suggests the possibility that both radiologists shared similar subjective thresholds in defining acceptable image quality. Hence, the observed similarity in their assessments is not unexpected.

A **B**
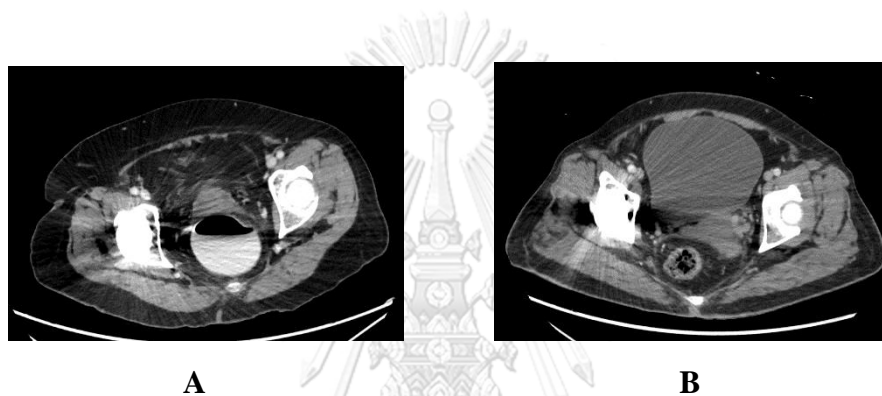
Figure 5.1 Transverse abdominal CT images obtained in a 78-year-old female weighing 60 kg with Metallic artifact from hip prosthesis by SECT(A), CT images obtained in a 66-year-old female weighing 50 kg with Metallic artifact from hip prosthesis by DECT VMI at 70 keV(B).

5.1.3 Radiation dose

5.1.3.1 The correlation between average $CTDI_{vol}$ and patient's effective

diameter

The major factor affecting $CTDI_{vol}$ from the correlation of effective diameter between both protocols is the tube current-time (mAs) as shown in Figure 4.6 of the CT whole abdomen in both protocols, since the mAs is proportional to the number of photons generated and the radiation doses received by patients. While the thickness and compositions of the body vary depending on the patient's size. As a result, the mAs is a dominant parameter for the radiation dose. The association of the $CTDI_{vol}$ in the entire abdomen CT between DECT and SECT was not statistically significant.

This study revealed that in DECT protocol, each effective diameter with a similar patient size corresponds to a comparable radiation dose, as illustrated in Figure 4.6, which is consistent with the findings of Topçuoğlu OM (13). The primary factor influencing $CTDI_{vol}$, in conjunction with BMI, for both protocols is likely the use of AEC in SECT. This is because the tube current is automatically increased to

accommodate greater patient thickness. Consequently, as patient thickness, BMI, and tube current rise, so does the radiation dose. In contrast, in DECT, the tube current remains constant and can be manually set by the user to remain consistent throughout the entire scan length for each effective diameter. Furthermore, CT parameters are maintained at a constant level based on the patient's weight (27). As a result, the distribution of effective diameter and $CTDI_{vol}$ in DECT exhibits a saturation effect compared to the SECT protocol.

5.1.3.2 Average CTDIvol between DECT and SECT protocols.

When comparing DECT and SECT protocol, the average $CTDI_{vol}$ of DECT was slightly different to 120 kVp under the same noise index (NI) based on individual patient weight, the specific protocol value used in emergency room at King Chulalongkorn Memorial Hospital. The radiation dose results obtained from both protocols were found to be within the limits of the diagnostic reference levels (DRLs) recommended by the AAPM's working group on standardization of CT nomenclature and protocols, as published in August, 2015 (28). Similar to the study conducted by Jeremy R. et al (3), our findings demonstrate that whole abdomen CT acquired using DECT has been provides equivalent or superior image quality compared to SECT while maintaining lower radiation doses.

This study has several limitations that should be acknowledged. Firstly, the sample size was relatively small, and the participants' body weight (range,45–75 kg) and body mass index (range, 15–30 kg/m^2) may not fully represent the diversity found in the Western population. Secondly, there was heterogeneity in some scan parameters within the SECT and DECT protocols, particularly the rotation time, where the SECT protocol used 0.5 s and the DECT protocol followed the default value of 0.6 s for the specific machine. Thirdly, although we administered the same injection rate and the contrast volume to each patient, the hemodynamic status of the patient could have potentially influenced the SNR in both DECT and SECT acquisitions. Lastly, only a rapid kVp fast switching dual- energy CT scanner from a single vendor was utilized. It is important to note that our findings are specific to contrast-enhanced abdominal CT, and results may differ when evaluating other types of DECT scans (e.g., non-contrast abdominal CT, DE CT pulmonary angiography, head CT). For future research, it is recommended to validate these findings on other CT scanners, conduct larger clinical studies with more diverse populations, and perform re-analyses considering additional body size metrics and radiation dose calculations. These efforts will contribute to a more comprehensive understanding of the study.

5.2 Conclusions

The findings of this study suggest that virtual monochromatic spectral images of 70 keV obtained from DECT on a rapid kVp-switching system provide higher vascular enhancement and image quality than SECT (120 kVp) portal-venous phase, when evaluating lesions in the whole abdomen CT examination. However, DECT has

higher image noise compared to 120 kVp, which did not affect the interpretation of radiologists. These results indicate that the DECT protocol for whole abdomen imaging can be used as a routine protocol in the emergency room, providing better objective image quality and unchanged subjective image quality comparable to conventional 120 kVp SECT.

จุฬาลงกรณ์มหาวิทยาลัย

CHULALONGKORN UNIVERSITY

REFERENCES

1.   Grajo J, Patino M, Prochowski Iamurri A, Sahani D. Dual Energy in Practice: Basic Principles and Applications. Applied Radiology. 2016;45:6-12.
2.   Wortman JR, Uyeda JW, Fulwadhva UP, Sodickson AD. Dual-Energy CT for Abdominal and Pelvic Trauma. Radiographics. 2018;38(2):586-602.
3.   Wortman JR, Shyu JY, Dileo J, Uyeda JW, Sodickson AD. Dual-energy CT for routine imaging of the abdomen and pelvis: radiation dose and image quality. Emerg Radiol. 2020;27(1):45-50.
4.   Johnson TR. Dual-energy CT: general principles. AJR Am J Roentgenol. 2012;199(5 Suppl):S3-8.
5.   Goo HW, Goo JM. Dual-Energy CT: New Horizon in Medical Imaging. Korean J Radiol. 2017;18(4):555-69.
6.   Faby S, Kuchenbecker S, Sawall S, Simons D, Schlemmer HP, Lell M, et al. Performance of today's dual energy CT and future multi energy CT in virtual non-contrast imaging and in iodine quantification: A simulation study. Med Phys. 2015;42(7):4349-66.
7.   Yu L, Leng S, McCollough CH. Dual-energy CT-based monochromatic imaging. AJR Am J Roentgenol. 2012;199(5 Suppl):S9-s15.
8.   Mileto A, Barina A, Marin D, Stinnett SS, Roy Choudhury K, Wilson JM, et al. Virtual Monochromatic Images from Dual-Energy Multidetector CT: Variance in CT Numbers from the Same Lesion between Single-Source Projection-based and Dual-Source Image-based Implementations. Radiology. 2016;279(1):269-77.
9.   Introduction to CT physics[online] 2004 [Available from: https://www.angelfire.com/nd/hussainpassu/Physics_of_Computed_Tomography.pdf.
10.   McCollough C, Edyvean S, Gould B, Keat N, Judy P, Kalender W, et al. The Measurement, Reporting, and Management of Radiation Dose in CT. AAPM Report. 2008;96.
11.   Goldman LW. Principles of CT: radiation dose and image quality. J Nucl Med Technol. 2007;35(4):213-25; quiz 26-8.
12.   Nagel H. CT Parameters that Influence the Radiation Dose. 2007. p. 51-79.
13.   Topcuoglu OM, Sarikaya B. Fast kilovoltage-switching dual-energy CT offering lower x-ray dose than single-energy CT for the chest: a quantitative and qualitative comparison study of the two methods of acquisition. Diagn Interv Radiol. 2019;25(3):204-9.
14.   Singh R, Sharma A, McDermott S, Homayounieh F, Rastogi S, Flores EJ, et al. Comparison of image quality and radiation doses between rapid kV-switching and dual-source DECT techniques in the chest. Eur J Radiol. 2019;119:108639.
15.   Body Size Thailand [Available from: http://waa.inter.nstda.or.th/stks/pub/2012/20120417-SizeThailand.pdf.
16.   Sugawara H, Takayanagi T, Ishikawa T, Katada Y, Fukui R, Yamamoto Y, et al. New Fast kVp Switching Dual-Energy CT: Reduced Severity of Beam Hardening Artifacts and Improved Image Quality in Reduced-Iodine Virtual Monochromatic Imaging. Acad Radiol. 2020;27(11):1586-93.
17.   Radcal-20CT20-Nested-CT-Phantom 2016 [Available from: https://radcal.com/20ct20-nested-ct-head-body-phantom/.

18.   Catphan ® 500 and 600 Manual [online] 2006 [Available from: file:///C:/Users/peng/Downloads/Catphan2B5002B6002BManual2B.831261131.pdf.

19.   Introduction of Radcal Accu-Gold+ [online] 2017 [Available from: https://radcal.com/wp-content/uploads/2016/11/Radcal-Accu-Gold-Plus-Brochure.pdf.

20.   Specification of The Chamber for Computed Tomography Dose Index (CTDI) [online] 2011 [Available from: https://radcal.com/wp-content/uploads/2016/10/radcal-10X6-3CT-chamber-spec-sheet.pdf.

21.   Noda Y, Goshima S, Nakashima Y, Miyoshi T, Kawai N, Kambadakone A, et al. Iodine dose optimization in portal venous phase virtual monochromatic images of the abdomen: Prospective study on rapid kVp switching dual energy CT. Eur J Radiol. 2020;122:108746.

22.   Kaza RK, Platt JF, Cohan RH, Caoili EM, Al-Hawary MM, Wasnik A. Dual-energy CT with single- and dual-source scanners: current applications in evaluating the genitourinary tract. Radiographics. 2012;32(2):353-69.

23.   Noda Y, Goshima S, Kozaka K, Yoneda N, Mizuno N, Kato A, et al. Optimal window settings in single-source dual-energy computed tomography of the abdomen. Eur J Radiol. 2018;109:204-9.

24.   Noda Y, Kawai N, Kawamura T, Kobori A, Miyase R, Iwashima K, et al. Radiation and iodine dose reduced thoraco-abdomino-pelvic dual-energy CT at 40 keV reconstructed with deep learning image reconstruction. Br J Radiol. 2022;95(1134):20211163.

25.   Matsumoto K, Jinzaki M, Tanami Y, Ueno A, Yamada M, Kuribayashi S. Virtual monochromatic spectral imaging with fast kilovoltage switching: improved image quality as compared with that obtained with conventional 120-kVp CT. Radiology. 2011;259(1):257-62.

26.   Yu L, Christner JA, Leng S, Wang J, Fletcher JG, McCollough CH. Virtual monochromatic imaging in dual-source dual-energy CT: radiation dose and image quality. Med Phys. 2011;38(12):6371-9.

27.   Kanal KM, Stewart BK, Kolokythas O, Shuman WP. Impact of operator-selected image noise index and reconstruction slice thickness on patient radiation dose in 64-MDCT. AJR Am J Roentgenol. 2007;189(1):219-25.

28.   Adult Routine Abdomen/Pelvis CT Protocols 2015 [updated 08/07/2015. Version 1.1:[Available from: https://www.aapm.org/pubs/ctprotocols/documents/adultabdomenpelvisct.pdf.

Appendix A: Data record form

Radiation Dose

CT scanner:										
Exam protocol:										
Patient information					Patient's scan record			Corrected diameter (cm)		
Patient No.	Age (y)	Gender (M/F)	Weight (Kg)	Height (cm)	Scan range (mm)	CTDI$_{vol}$ (mGy)	DLP (mGy.mm)	AP	LAT	ED

CT Number (HU) and noise (SD) measurement

CT scanner:														
Exam protocol:														
Patient information					Organ	CT Number (HU)			Average	SD			Average	
Patient No.	Age (y)	Gender (M/F)	Weight (Kg)	Height (cm)		1	2	3		1	2	3		
					Aorta									
					MPV									
					Liver									
					Spleen									
					Psoas									
					Aorta									
					MPV									
					Liver									
					Spleen									
					Psoas									
					Aorta									
					MPV									
					Liver									
					Spleen									
					Psoas									
					Aorta									
					MPV									
					Liver									
					Spleen									
					Psoas									
					Aorta									
					MPV									
					Liver									
					Spleen									
					Psoas									

APPENDIX B: Quality Control of Computed Tomography system

1. Mechanical accuracy
1.1 Alignment of table to gantry

Purpose: To ensure that long axis of the table is horizontally aligned with a vertical line passing through the rotational axis of the scanner.

Methods:

1. Locate the table midline using a ruler and mark it on a tape affixed to the couch.

2. Extend the table top into gantry to tape position.

3. Measure the horizontal deviation between the gantry aperture center and the table midline.

Tolerance: The deviation should be less than 5 mm.

Results:

Table B-1: Results of alignment of table to gantry.

	Table	Gantry
Distance from Right to Centre (mm)	213	398
Distance from Centre to Left (mm)	212	399
Measured Deviation	0.5	0.5

Measured deviation: (Distance from right to center – Distance from center to left)/2

Comments: Pass

1.2 Scan localization light accuracy

Purpose: To test congruency of scan localization light and scan plane.

Method:

1. Place the tape measurement vertically along the midline of the couch aligned with the longitudinal axis as Figure B-1.

Figure B-1. The measurement of scan localization light accuracy.

2. Set external light align with the reference point on the tape measurement.

3. Set table position to zero. Move table by monitor scanner, the table position moves from external to internal localization light. Measure and record deviation position.

Tolerance: Differentiation of the marker between external and internal laser should exceed 2 mm.

Table B-2: Scan localization light accuracy

Measured Deviation	External	0 cm
	Internal	0 cm

Comment: Pass

1.3 Table increment accuracy.

Purpose: To determine the accuracy and reproducibility of table longitudinal motion.

Method: 1. Tape a measuring tape at the foot end of the table.

2. Set the number of measuring tape to be the center of the tape to function as an indicator.

3. Load table with 70-80 kg, e.g., have assistant lie on table.

4. From the initial position move the table to 300, 400 and 500 mm into the gantry under software control.

5. Record the relative displacement of the pointer the ruler.

6. Reverse the direction of the table and record the value.

Tolerance: Positional error should be less than 3 mm.

Results:

Table B-3: Results of table increment accuracy.

| Indicated(mm.)	Measured(mm.)	Deviation(mm.)
300	300	0
400	400	0
500	500	0
-300	300	0
-400	400	0
-500	500	0

Deviation = | Indicated – Measured|

Comment: Pass

2.Image performance

2.1 Position dependence and S/N ratio of CT numbers

Method:

1. Position the CT head phantom centered in the gantry.

2. Using 10 mm slice thickness obtain one scan using typical head technique.

3. Select a circular region of interest of approximately 400 sq. mm.

4. Record the mean C.T. number and standard deviation for each of the positions 1 through 5. Technique: 120 kV, 300 mA, 1 second, 250 mm. FOV
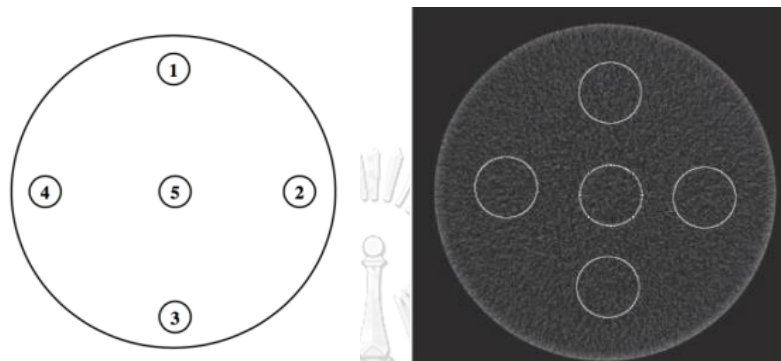
Figure B-2. Draw region of interest for each of the positions 1 through 5.

Tolerance: The coefficient of variation (COV) should be less than 0.2

Results:

Table B-4: Position dependence and S/N ratio of C.T. numbers

Position	Mean C.T. #	S.D.	C.V.	COV
1	7.26	3.13	0.43	-
2	7.13	3.16	0.44	0.005
3	7.16	2.89	0.40	0.05
4	7.21	3.16	0.44	0.05
5	7.16	2.89	0.40	0.045

Comments: Pass

2.2 Reproducibility of CT. Number

Methods:

1. Using the same set up and parameter setting as position dependence, obtain four scans.
2. Using the same ROI as position dependence in center of the phantom.
3. Obtain mean C.T. numbers for each of the four scans.

Tolerance: The coefficient of variation of mean C.T number should be less than 0.002

Technique: Single energy: 120 kVp, 300 mAs, FOV 250 mm.

Results:

Table B-5: Results of reproducibility of CT numbers.

Run Number	1	2	3	4
Mean C.T #	9.60	9.41	9.29	9.52
Mean Global C.T Number	9.46			
Standard Deviation	0.013			
Coefficient of variation	0.0019			

Comments: Pass

จุฬาลงกรณ์มหาวิทยาลัย

CHULALONGKORN UNIVERSITY

2.3 mAs Linearity

Methods:

1. Set up PMMA head phantom at the center of gantry.
2. Insert 10 cm long pencil chamber in the center slot of the phantom.
3. Select the same kVp and time as used for head scan.
4. Obtain four scans in each of the mA station normally used in the clinic.
5. For each mA, record the exposure in mGy for each scan.
6. Scan should be performed in the increasing order of mA.
7. Compute mGy/mAs for each mA setting.

Technique: 120 kVp, 1.0 sec, FOV 250 mm, varying mA. Detector configuration 64 x 0.625 mm

Results:

Table B-6: Results of mAs linearity.

| mAs	Exposure in mGy			Average (mGy)	mGy/mAs	CV
	Run 1	Run 2	Run 3			
100	5.174	5.169	5.172	5.16	0.052	-
200	10.23	10.24	10.24	10.24	0.051	0.005
300	15.36	15.35	15.35	15.35	0.051	0
400	20.75	20.74	20.64	20.71	0.052	0.006
500	25.77	25.78	25.78	25.78	0.052	0.002
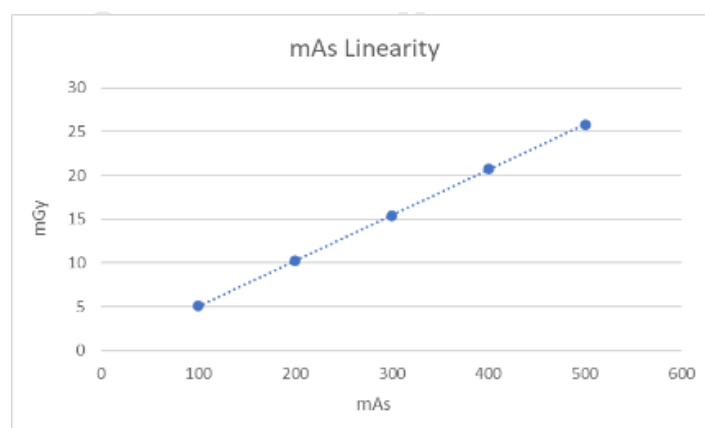
Figure B-3 The correlation of mGy and mAs.

Comment: Pass
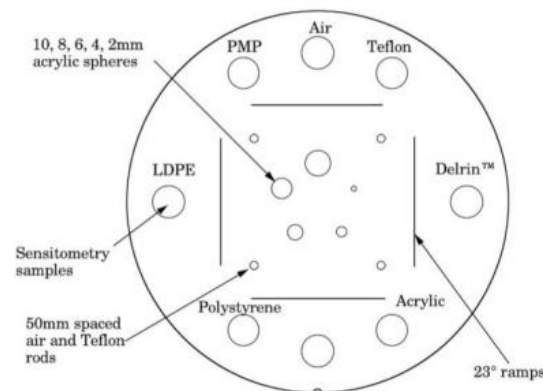
2.4. Linearity of CT. Numbers

Methods.

1. Set up CATPHAN® 600 phantom in beam alignment as shown in Figure B-4.
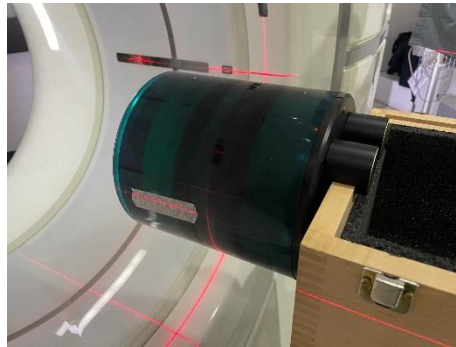
Figure B-4 The position of CATPHAN® 600 phantom

2. Select section 1 of the Catphan® 600 phantom which containing the test objects of different C.T numbers (CTP404, sensitometer and pixel size module) as shown in Figure B-5.

Figure B-5 The section containing the test objects of different CT numbers.

3. Select the head technique and parameter setting as followings:

120 kVp, 300 mA, 1 sec, 300 mm FOV

4. Draw ROI of sufficient size to cover the test objects and place in middle of each object.

5. Record the CT number of each object and record position of table at the center of section 1.

Tolerance: R-square value between measured C.T. number and linear attenuation coefficient (μ) more than 0.9

Results:

Table B-7: Results of linearity of CT number.

Material	μ	Nominal CT Number	Measured CT Number
Acrylic	0.215	120	120.49
Polystyrene	0.188	-35	-43.73
LDPE	0.174	-100	-101.59
PMP	0.157	-200	-188.67
Delrin	0.245	340	296.41
Teflon	0.363	990	883.99
Air (inferior)	0	-1000	-1000.32
Air (superior)	0	-1000	-996.78
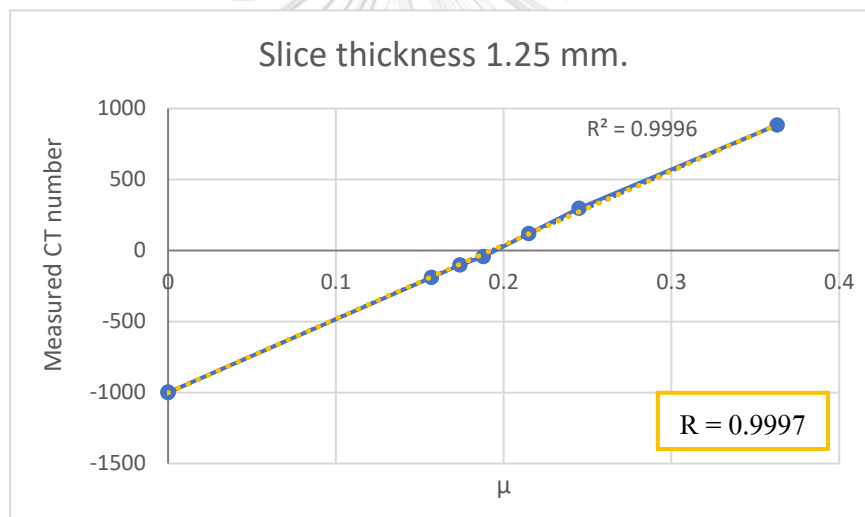
Comment: Pass

2.5 Accuracy of Distance Measurement

Methods:

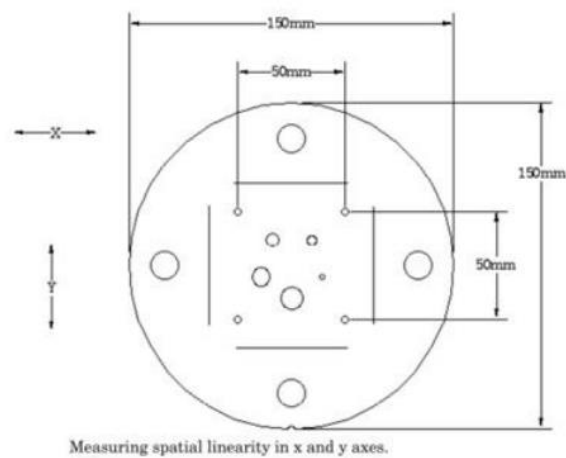1. Set up the CATPHAN® 600 phantom in beam alignment.

2. Select the section containing the test accuracy of distance measurement (CTP404, sensitometer and pixel size module).

3. Select head technique and the same parameter setting as linearity of CT number measurement.

4. Measure object in x and y axes as shown in Figure B-7.

Figure B-7 Measuring spatial linearity in x and y axis.

Tolerance: Difference between indicated and measured should be less than 3 mm.

Results:

Table B-8: Results of accuracy of distance measurement.

| Indicated distance (mm)	Indicated (mm)	Measured distance (mm)	Difference (mm)
150 mm X)	150	151.04	-1.04
150 mm (Y)	150	150.75	-0.75
50 mm (vertical)	50	50.06	-0.06
50 mm (horizontal)	50	50.92	-0.92

Difference = | Indicated – Measured |

Comments: Pass

2.6 High Contrast Resolution

Methods:

1. Set up CATPHAN® 600 phantom as described in beam alignment.

2. Select the section of Catphan600 phantom which containing the high contrast resolution test object. (CTP528, 21 line pair high resolution, distance) as shown in Figure B-8.
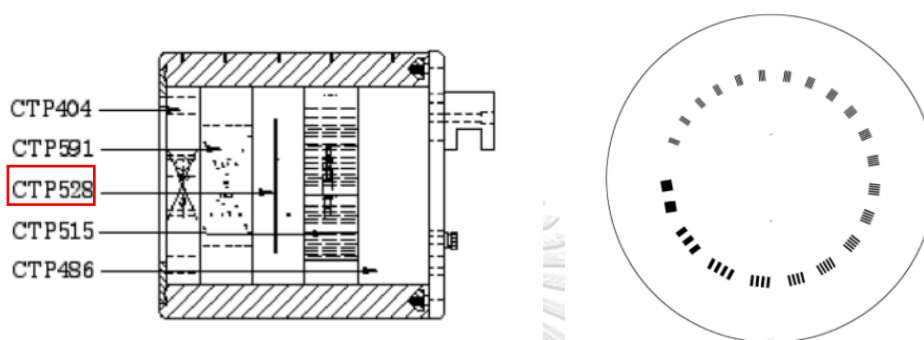
Figure B-8 The module of high contrast resolution test object

3. Select the head technique and the same parameter setting as linearity of CT number measurement.

4. Select the area containing the high contrast resolution test objects and adjust appropriate window and level for the best visualization of the test objects and magnify as necessary.

5. Record the smallest test object visualized on the monitor.

Technique: kVp: 120 mA: 300Seconds: 1.0 FOV: 300 mm Slice Thickness: 1.25, 2.5, 5 mm

Tolerance: Should be more than 5-line pairs/cm

Results:

Table B-9: Results of high contrast resolution.

| Slice Thickness in mm	Resolution (lp/cm)	Gap size
1.25 mm	8	0.063 cm
2.5 mm	8	0.063 cm
5 mm	8	0.063 cm

Comments: Pass

2.7 Low contrast Resolution

Methods:

1. Set up the CATPHAN® 600 phantom as described in beam alignment.

2. Select the head technique and the same parameter setting as linearity of CT number measurement.

3. Select the section containing the low contrast resolution test object. (CTP515, sub-slice and supra-slice low contrast.) as shown in Figure B-9.
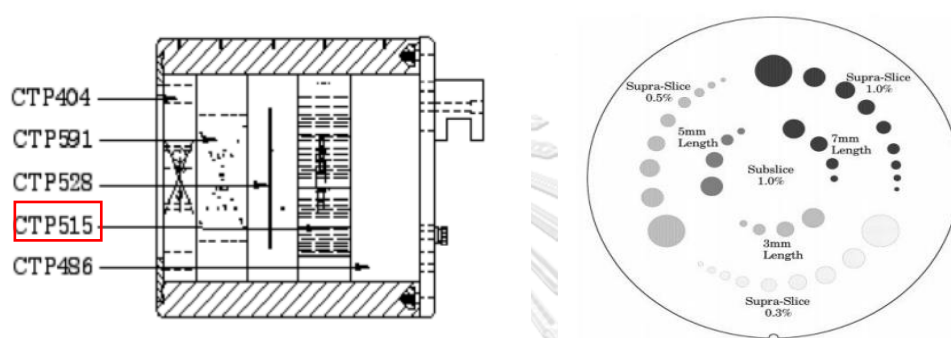
Figure B-9 The module of low contrast resolution test object

4. Select appropriate window and level for the best visualization of the test objects.

5. Record the smallest test object visualized.

Technique: 120 kVp, 300 mA, 1 sec, 240 mm FOV, thickness 3, 5, 7 mm.

Tolerance: The smallest diameter hole 7 mm (4 holes) should be seen at 0.5% contrast

Results:

Table B-10: Results of low contrast resolution.

Slice thickness in mm	Visualized smallest spokes					
	Contrast level of supra-slice			Length of sub-slice		
	1.00%	0.50%	0.30%	7 mm	5 mm	3 mm
1.25	7	5	2	3	3	2
2.5	8	6	5	4	3	3
5	9	7	6	4	3	3

Comments: Pass

2.8 Slice Thickness Accuracy (Slice Width)

Method:

1. Set up the phantom as described in beam alignment set up similar to beam profile measurement.

2. Select the section containing the accuracy of the slice thickness test objects (CTP404 slice width Module) as shown in Figure B-10.
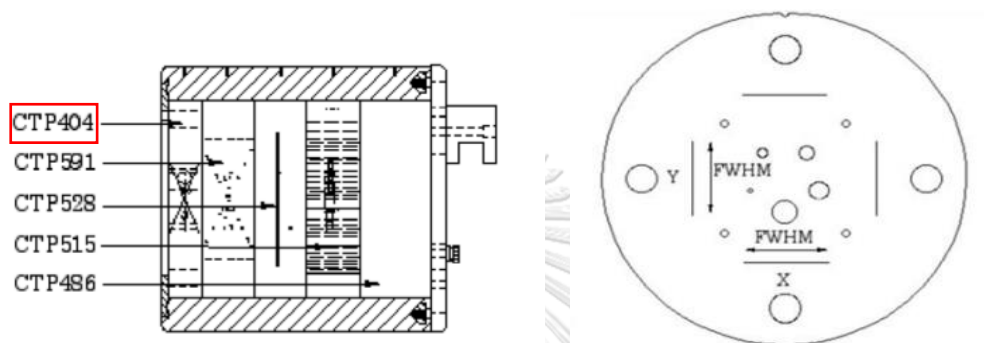
Figure B-10. The module of slice thickness accuracy test object

3. Select the head technique, 120 kVp, 300 mAs, smallest slit width.

4. Perform several scans with different programmed slice thicknesses under auto control.

5. Perform scan following Catphan manual in each slice thickness.

6. Calculate the real slice thickness

   6.1 Draw ROI to identify mean CT number of the area adjacent to the wire ramp for define as

   "Background"

   6.2 Adjust window width to 1.
   6.3 Move window level to the point where the wire ramp disappears.
   6.4 Determine window level at this position is "Maximum value."
   6.5 Define the half maximum CT by:
   ➢ Net peak CT = Maximum value – Background
   ➢ 50% Net peak CT = $\frac{Net\ peak\ CT}{2}$
   ➢ Half maximum CT = 50% Net peak CT + Background
   6.6 Adjust window level to be equal at half maximum CT.
   6.7 Draw line along the ramp that show length of each ramp.
   6.8 Average length of 4 wire ramp as FWHM.
   6.9 Slice width = FWHM x 0.42

Tolerance: The deviation should be less than 1 mm

Result:

Table B-11 Slice thickness accuracy.

Slice Thickness (mm)	1.25	2.5	5
Peak	621	345	220
BG	92.76	94.71	95.93
Net peak (NP)	528.24	250.29	124.07
50% (NP)	264.12	125.15	62.04
HM (50%NP+BG)	356.88	219.86	157.97
FWHM L1	2.92	6.52	13.15
FWHM L2	3.02	6.41	13.59
FWHM L3	2.86	6.41	13.6
FWHM L4	2.81	6.24	12.86
Average FWHM	2.9	6.4	13.3
SL=Avg FWHM x 0.42	1.22	2.69	5.59
Diff (calculate-set)	-0.03	0.19	0.59

Slice Thick in mm.	Measured (mm)	Deviation (mm)
1.25	1.22	-0.03
2.5	2.69	0.19
5	5.59	0.59

Comment: Pass

2.9. Image Uniformity

Methods:

1. Set up the CATPHAN® 600 phantom as described in beam alignment.

2. Select the section6 (CTP 486, Solid image uniformity module) used to estimate image uniformity.

3. Select the head technique and the same parameter setting as linearity of CT number measurement.

4. Draw ROI of approximately 400 mm^2 and place in the middle and peripheral of the phantom in each slice thickness as illustrated in Figure B-11.
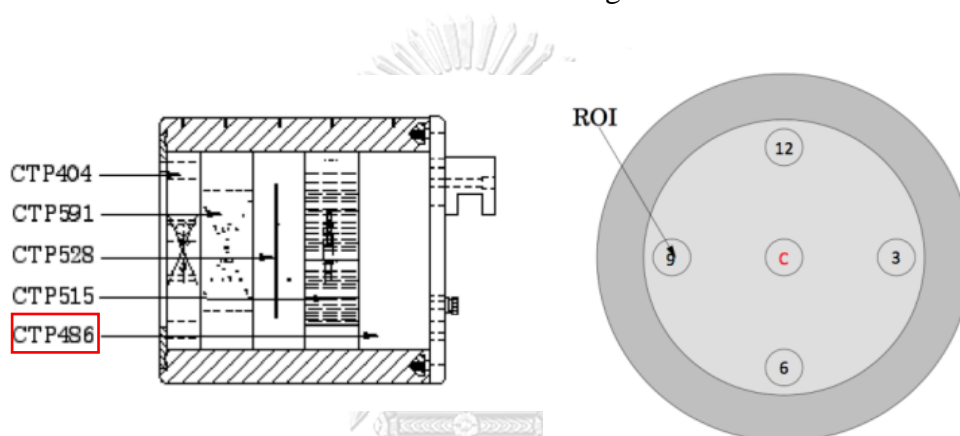
Figure B-11 The measurement of image uniformity

5. Record the mean C.T number of middle and peripheral of the phantom.

Tolerance: Difference should be less than 5 HU.

Results:

Table B-12: Image uniformity

Position	Mean C.T Number	S.D.	Difference (HU)
1	9.82	3.29	0
2	8.07	3.12	1.75
3	7.8	2.96	2.02
4	8.05	3.01	1.77
5	7.93	2.95	1.89

Different of C.T. Number = | Mean C.T number at center – Mean C.T. number at peripheral |

Comments: Pass

3.Verification of Computed Tomography Dose Index (CTDI)

3.1 Measurement of $C_{a,100}$ free in air (CTDI$_{air}$)

Purpose: To verification of Computed Tomography Dose Index (CTDI)

Method:

1. Set the 100 mm pencil chamber at the iso-center of the CT bore.

2. Using head and body protocols.

3. Set scan parameter at 100 mA, 1 sec scan time.

4. Change kilovoltage at 80, 100, 120 and 140.

5. Record CT dose in unit of mGy.

Figure B-12 CTDI$_{100}$ in air measurement using 100 mm pencil ion chamber.

Result:

Table B-13: The measured CTDI$_{100}$ in air for head protocol

Parameters	kVp			
	80	100	120	140
Meter reading (mGy)	4.158	6.84	9.948	13.43
$C_{a,100}$ (mGy)	0.013	0.021	0.031	0.042
$_nC_{a,100}$ (mGy/mAs)	0.00013	0.00021	0.00031	0.00042
CTDI$_{vol}$ on console reading (mGy)	5.45	9.87	15.1	21.23
DLP on console reading (mGy.cm)	21.79	39.49	60.39	84.92
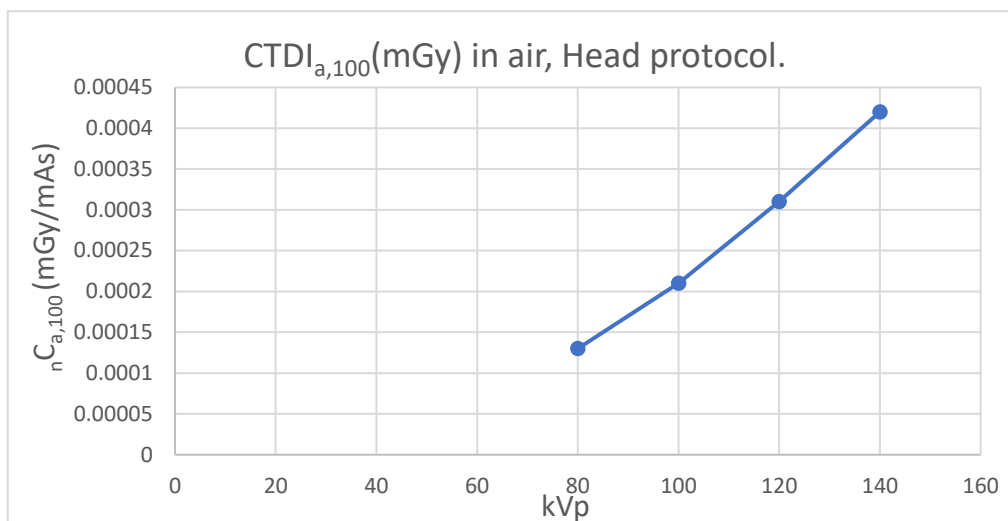
Figure B-13 CTDI$_{100}$ in air for head protocol.

Table B-14 The measured CTDI$_{100}$ in air for body protocol with 500 mm FOV (L).

Parameters	kVp			
	80	100	120	140
Meter reading (mGy)	2.86	5.09	7.79	12.91
C$_{a,100}$ (mGy)	0.009	0.016	0.024	0.034
$_n$C$_{a,100}$ (mGy/mAs)	0.00009	0.00016	0.00024	0.00034
CTDI$_{vol}$ on console reading (mGy)	2.15	4.22	6.8	9.9
DLP on console reading (mGy.cm)	8.61	16.87	16.87	39.59
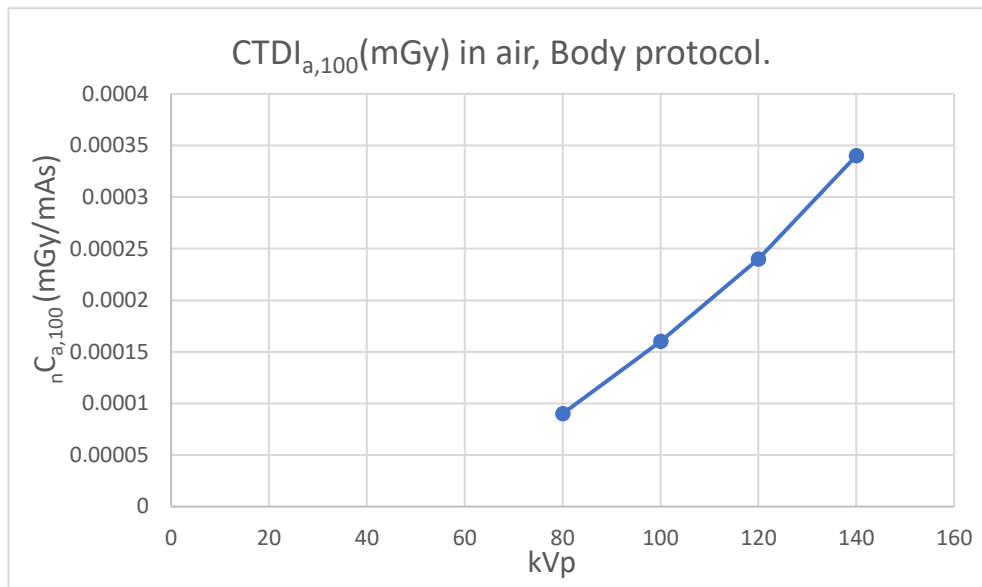
Figure B-14 CTDI$_{100}$ in air for body protocol.

3.2 Measurement of CTDI$_{100}$ in PMMA phantom

Purpose: To verification of Computed Tomography Dose Index (CTDI)

Method:

1. The CTDI$_{100}$ in head and body PMMA phantom by using a 100 mm pencil chamber placed in each hole of 16 and 32 cm diameter PMMA phantom for head and body protocols at the iso-center of C.T. bore.

2. Using head and body protocols.

3. The scan parameters were 100 mA, 1 sec scan time, 180 and 500 mm FOV for all measurements at each kVp setting of 80, 100, 120 and 140 in axial volume mode.

4. Record C.T. dose in unit of mGy.

5. Calculate C$_w$ and $_n$C$_w$ following

$$C_w = \frac{1}{3}\left(C_{PMMA,100,\,C} + 2C_{PMMA,100,\,P}\right)$$

$$_nC_w = \frac{C_w}{P_{lt}}$$

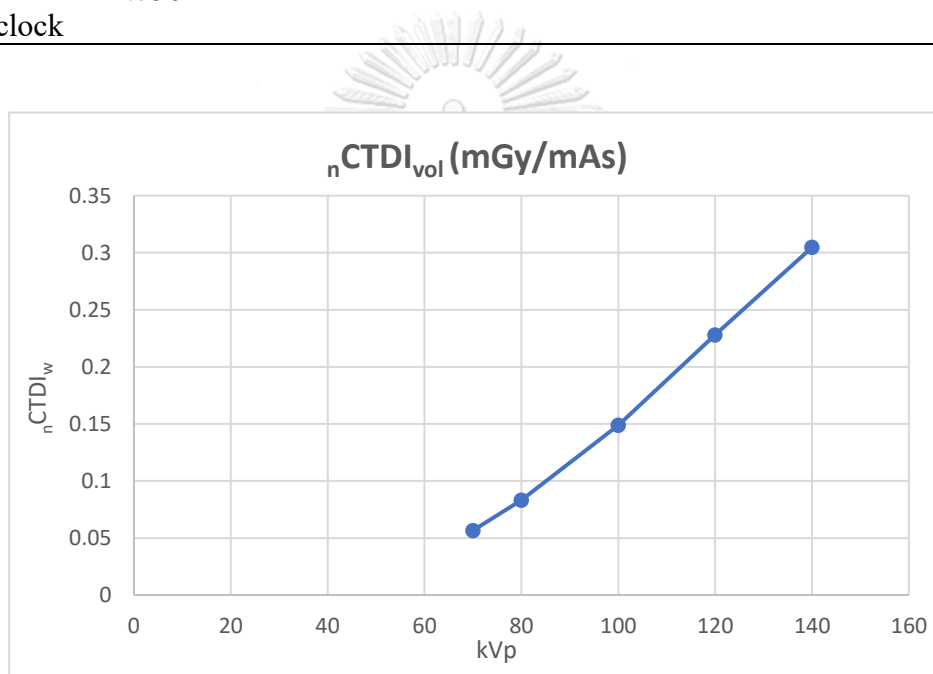**Tolerance**: CTDI$_{100}$ measurements in a PMMA phantom is ±10%.

Results:

Table B-15 $CTDI_{100}$ measurement in head PMMA phantom.

			80 kVp			
Position	Meter reading (mGy)	$C_{PMMA,100}$ (mGy)	$CTDI_w$ (mGy)	$_nCTDI_w$ (mGy/mAs)	$CTDI_{vol}$ (mGy)	$_nCTDI_{vol}$ (mGy/mAs)
Center	0.9651	7.302				
3 o'clock	0.4422					
6 o'clock	0.4159	8.848	8.33	0.0833	8.33	0.0833
9 o'clock	0.4391					
12 o'clock	0.4723					

			100 kVp			
Position	Meter reading (mGy)	$C_{PMMA,100}$ (mGy)	$CTDI_w$ (mGy)	$_nCTDI_w$ (mGy/mAs)	$CTDI_{vol}$ (mGy)	$_nCTDI_{vol}$ (mGy/mAs)
Center	0.6807	13.614				
3 o'clock	0.7849					
6 o'clock	0.736					
9 o'clock	0.7717	15.591	14.932	0.149	14.932	0.149
12 o'clock	0.8256					

			120 kVp			
Position	Meter reading (mGy)	$C_{PMMA,100}$ (mGy)	$CTDI_w$ (mGy)	$_nCTDI_w$ (mGy/mAs)	$CTDI_{vol}$ (mGy)	$_nCTDI_{vol}$ (mGy/mAs)
Center	1.065	21.3				
3 o'clock	1.166					
6 o'clock	1.132	23.505	22.77	0.228	22.77	0.228
9 o'clock	1.166					
12 o'clock	1.237					

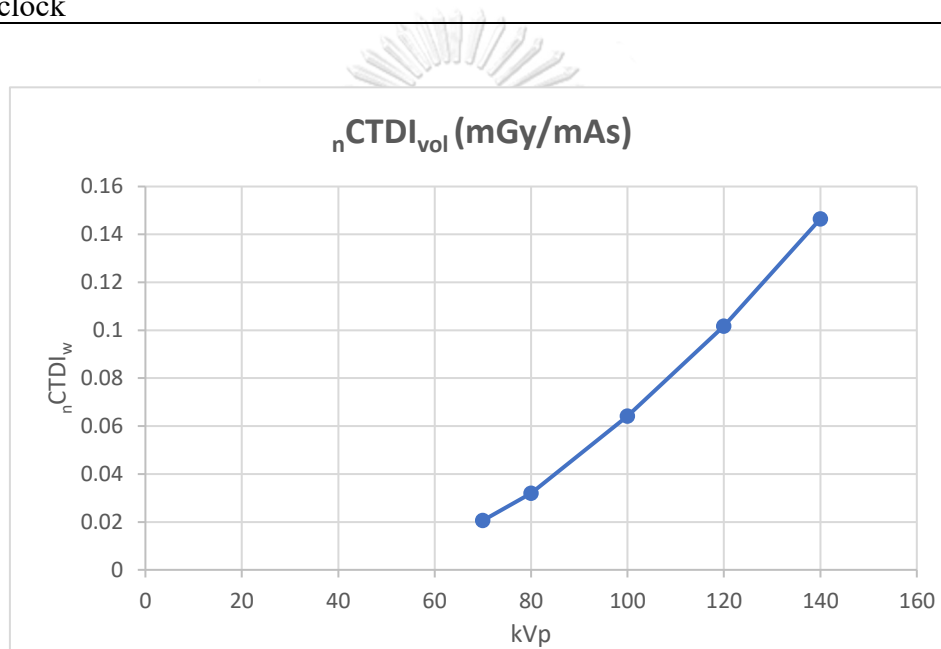| 140 kVp						
Position	Meter reading (mGy)	$C_{PMMA,100}$ (mGy)	$CTDI_w$ (mGy)	$_nCTDI_w$ (mGy/mAs)	$CTDI_{vol}$ (mGy)	$_nCTDI_{vol}$ (mGy/mAs)
Center	1.495	29.9				
3 o'clock	1.246					
6 o'clock	1.56	30.775	30.483	0.3048	30.483	0.3048
9 o'clock	1.613					
12 o'clock	1.736					

Figure B-15 $CTDI_{100}$ measurement in head PMMA phantom.

Table B-16 $CTDI_{100}$ measurement in body PMMA phantom with 500 mm FOV (L).

80 kVp

Position	Meter reading (mGy)	$C_{PMMA,100}$ (mGy)	$CTDI_w$ (mGy)	$_nCTDI_w$ (mGy/mAs)	$CTDI_{vol}$ (mGy)	$_nCTDI_{vol}$ (mGy/mAs)
Center	0.0797	1.594				
3 o'clock	0.2006					
6 o'clock	0.1846					
9 o'clock	0.2065	3.993	3.194	0.0319	3.194	0.0319
12 o'clock	0.207					

100 kVp

Position	Meter reading (mGy)	$C_{PMMA,100}$ (mGy)	$CTDI_w$ (mGy)	$_nCTDI_w$ (mGy/mAs)	$CTDI_{vol}$ (mGy)	$_nCTDI_{vol}$ (mGy/mAs)
Center	0.1754	3.508				
3 o'clock	0.4075					
6 o'clock	0.3579					
9 o'clock	0.4009	7.869	6.415	0.0642	6.415	0.0642
12 o'clock	0.4074					

120 kVp

Position	Meter reading (mGy)	$C_{PMMA,100}$ (mGy)	$CTDI_w$ (mGy)	$_nCTDI_w$ (mGy/mAs)	$CTDI_{vol}$ (mGy)	$_nCTDI_{vol}$ (mGy/mAs)
Center	0.3003	6.006				
3 o'clock	0.6184					
6 o'clock	0.563					
9 o'clock	0.644	12.255	10.172	0.1017	10.172	0.1017
12 o'clock	0.6252					

140 kVp

Position	Meter reading (mGy)	$C_{PMMA,100}$ (mGy)	$CTDI_w$ (mGy)	$_nCTDI_w$ (mGy/mAs)	$CTDI_{vol}$ (mGy)	$_nCTDI_{vol}$ (mGy/mAs)
Center	0.4524	9.048				
3 o'clock	0.8881					
6 o'clock	0.8314	17.451	14.65	0.1465	14.65	0.1465
9 o'clock	0.8855					
12 o'clock	0.8852					

Figure B-16 $CTDI_{100}$ measurement in body PMMA phantom

Comments: Pass

3.3 CTDI$_{vol}$ on monitor and calculated CTDI$_{vol}$

Purpose: To compare the CTDI$_{vol}$ displayed on CT monitor with calculated CTDI$_{vol}$.

Methods:

1. Determine the CTDI$_{vol}$ by using the results in Table B-15 and B-16.

2. The CTDI$_{vol}$ displayed on CT monitor were recorded to compare percentage difference with the calculated values as shown in Table B-17 for CTDI$_{vol}$ in head phantom and table B-18 for CTDI$_{vol}$ in body phantom.

Tolerance: The difference between measured CTDI$_{vol}$ and display should be less than ±10%

Results:

Table B-17 CTDI$_{vol}$ displayed on monitor and calculated CTDI$_{vol}$ in head phantom using head techniques: 100 mAs, and 180 mm FOV.

kVp	CTDI$_{vol}$ (mGy) in 16 cm head phantom		
	Calculated CTDI$_{vol}$	Displayed CTDI$_{vol}$	% Difference
80	8.33	8.19	-1.722
100	14.93	14.84	-0.618
120	22.77	22.69	-0.352
140	30.48	31.91	4.57
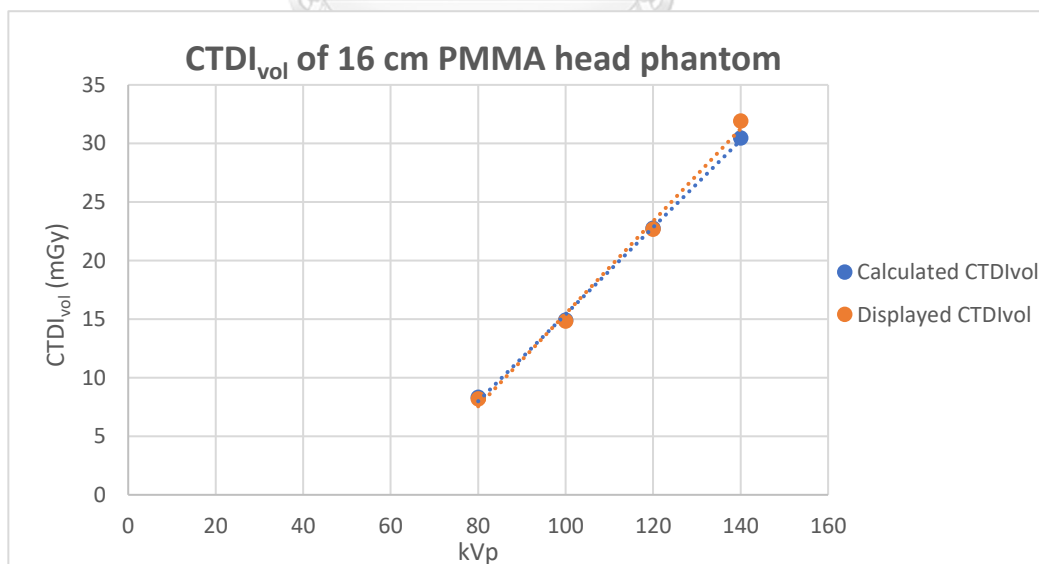
Figure B-17 CTDI$_{vol}$ on monitor and calculated CTDI$_{vol}$ in 16 cm PMMA head phantom.

Table B-18 CTDI$_{vol}$ displayed on monitor and calculated CTDI$_{vol}$ in body phantom using body techniques: 100 mAs, and 500 mm FOV.

kVp	CTDI$_{vol}$ (mGy) in 32 cm body phantom		
	Calculated CTDI$_{vol}$	Displayed CTDI$_{vol}$	% Difference
80	3.19	3.21	0.506
100	6.42	6.29	-1.968
120	10.17	10.14	-0.3151
140	14.65	14.77	0.8158
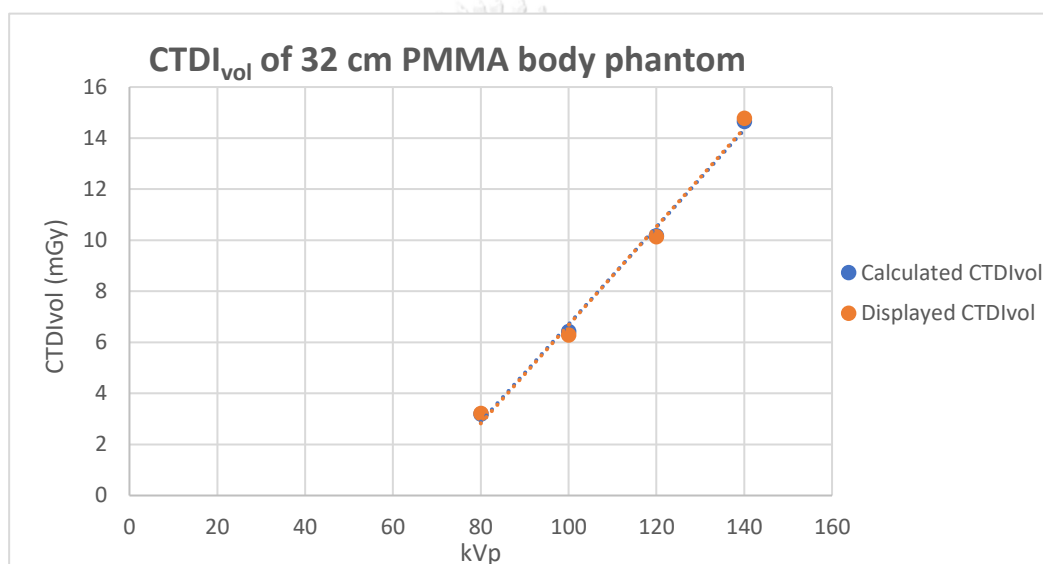
Figure B-18 CTDI$_{vol}$ on monitor and calculated CTDI$_{vol}$ in 32 cm PMMA body phantom.

Comment: Pass

APPENDIX C

The approval of institutional review board

COA No. 1197/2022

IRB No. 0415/65

INSTITUTIONAL REVIEW BOARD

Faculty of Medicine, Chulalongkorn University

1873 Rama 4 Road, Pathumwan, Bangkok 10330, Thailand, Tel 662-256-4493

Certificate of Expedited Review Approval

(COA No. 1197/2022)

The Institutional Review Board of the Faculty of Medicine, Chulalongkorn University, Bangkok, Thailand, has approved the following study in compliance with the International guidelines for human research protection as Declaration of Helsinki, The Belmont Report, CIOMS Guideline and International Conference on Harmonization in Good Clinical Practice (ICH-GCP)

Study Title : Comparison of radiation dose and image quality between fast kVp switching dual-energy CT and routine single-energy CT for whole abdomen at King Chulalongkorn Memorial Hospital

Study Code : -

Principal Investigator : Miss Chanthawan Khemkhangboon

Affiliation of PI : Department of Radiology, Faculty of Medicine, Chulalongkorn University.

Review Method : Expedited

Continuing Report : At least once annually or submit the final report if finished.

Document Reviewed :
1. Research Proposal Version 2 Date 26 Aug 2022
2. Protocol Synopsis Version 1 Date 6 Jun 2022
3. Case Record Form Version 1 Date 6 Jun 2022

Approval granted is subject to the following conditions: (see back of this Certificate)

VITA

NAME	Ms. Chanthawan Khemkhangboon
DATE OF BIRTH	21 October 1991
PLACE OF BIRTH	Nan, Thailand
INSTITUTIONS ATTENDED	Bachelor of Science (Radiological Technology), Faculty of Science, Ramkhamhaeng University, Bangkok, Thailand, 2019
HOME ADDRESS	122/3, RAMA2 Road, Phanthai Norasing, Mueang Samut Sakhon, Samut Sakhon 74000, Thailand.
PUBLICATION	Khemkhangboon C, Yuenyongsinchai K, Pisuchpen N, Khamwan K. Comparison of radiation dose and image quality between fast-kV switching DECT and SECT for whole-abdominal CT examination. The 14th Annual Scientific Meeting of Thai Medical Physicist Society, 27-29 January 2023, Nan, Thailand. pp. 182-185.

จุฬาลงกรณ์มหาวิทยาลัย
CHULALONGKORN UNIVERSITY